# Variational Retrieval of Cloud Parameters from GOES Sounder Longwave Cloudy Radiance Measurements

JUN LI

*Cooperative Institute for Meteorological Satellite Studies, University of Wisconsin—Madison, Madison, Wisconsin*

W. PAUL MENZEL

*Office of Research and Applications, NOAA/NESDIS, Madison, Wisconsin*

ANTHONY J. SCHREINER

*Cooperative Institute for Meteorological Satellite Studies, University of Wisconsin—Madison, Madison, Wisconsin*

(Manuscript received 7 February 2000, in final form 27 July 2000)

ABSTRACT

The optimal nonlinear inversion or one-dimensional variational (1DVAR) method was used to retrieve the cloud-top height and effective cloud amount from Geostationary Operational Environmental Satellite (GOES) sounder longwave spectral-band cloudy radiance measurements. The cloud-top pressure and effective cloud amount derived from the carbon dioxide ($CO_2$)–slicing technique served as the background or first guess in the 1DVAR retrieval process. The atmospheric temperature profile, moisture profile, and surface skin temperature from the forecast analysis were used for the radiative transfer calculation in both the $CO_2$-slicing method and the 1DVAR retrieval processing. Simulation studies were made to investigate the accuracy (the retrievals were compared with truth) of the cloud-top pressures and the effective cloud amounts derived from both the $CO_2$-slicing and 1DVAR algorithms. Significant improvement of 1DVAR over $CO_2$-slicing cloud properties was found in the simulation studies; an improvement of 10–50 hPa for root-mean-square error was obtained in 1DVAR over the $CO_2$-slicing-derived cloud-top pressures, depending on the cloud height (high, mid, or low). This improvement came largely from the reduction of the bias in the 1DVAR retrievals over the $CO_2$-slicing cloud-top pressures. The 1DVAR approach was applied to process the *GOES-8* sounder cloudy radiance measurements; consistent with the simulation results, $CO_2$ slicing assigned high and low clouds to lower levels than 1DVAR did.

## 1. Introduction

Clouds play an important role in the earth's water and energy budgets. Their impact on the radiation budget can result in a heating or a cooling of the planet, depending on the radiative properties of the cloud and its altitude (Stephens and Webster 1981; Stephens et al. 1990). Cloud parameters, such as cloud-top height and fractional cloud coverage and emissivity, are useful in numerical weather prediction (NWP) (Diak et al. 1998; Bayler et al. 2000; Kim and Benjamin 2000). A significant advance in NWP has been the estimation of cloud motion vectors from sequences of geostationary satellite images (Velden et al. 1997) and the assignment of heights or pressures to these vectors (Eyre and Menzel 1989).

Many schemes have been proposed for estimating cloud parameters from the data of imaging and sounder radiances (Isaacs et al. 1986). Recently, schemes include the minimum residual method (Wielicki and Coakley 1981; Susskind et al. 1987; Eyre and Menzel 1989). One important passive remote sensing method for obtaining the altitude of mid- and upper-level clouds, especially transmissive clouds, is the carbon dioxide ($CO_2$)–slicing technique (Chahine 1974; Smith et al. 1974; Smith and Platt 1978; Menzel et al. 1983, 1992). The advantage of the minimum residual method is that it can be applied with any combination of two or more spectral bands, and the disadvantage is that the solution might be unstable because of the ill-posed radiative transfer inversion problem (Li and Huang 1999). The advantage of the $CO_2$-slicing technique is that each of the longwave infrared sounding spectral bands has vary-

*Corresponding author address:* Dr. Jun Li, CIMSS/SSEC, University of Wisconsin—Madison, 1225 West Dayton St., Madison, WI 53706.
E-mail: junl@ssec.wisc.edu

ing opacity to $CO_2$ gas, thereby causing each spectral band to be sensitive to a different layer in the atmosphere. The method has been shown to be effective for single-layer, nonblack, mid- to high-level clouds, such as cirrus (Baum and Wielicki 1994). The disadvantage of the $CO_2$-slicing method is that it selects only two spectral bands to obtain a solution (the spectral band pair used depends on the cloud altitude). Errors can be large in some specific atmospheric conditions, such as in the presence of a low-level temperature inversion, thin, high clouds, low clouds, and multilayer clouds. Because the one-dimensional variational (1DVAR) method uses the $CO_2$-slicing cloud product as constraint (the first guess) and uses all longwave spectral bands in the inversion procedure, it takes the advantages of $CO_2$-slicing and minimal residual methods while overcoming the disadvantages of the $CO_2$-slicing technique (using two spectral bands for solution) and the minimal residual method (unstable solution).

By satellite infrared remote sensing, cloud properties can be measured with high spatial and temporal resolution. Previous investigators have applied the $CO_2$-slicing technique to relatively low spatial or temporal resolution data such as that from the High-Resolution Infrared Sounder (Smith et al. 1979; Wylie and Menzel 1999) and the Visible–Infrared Spin Scan Radiometer Atmospheric Sounder (Menzel et al. 1992).

Since April 1994, the new generation of Geostationary Operational Environmental Satellite (GOES) (Menzel and Purdom 1994) sounders are providing higher spatial and temporal resolution measurements for deriving atmospheric parameters such as temperature, moisture, cloud-top pressure (CTP; Menzel et al. 1998), sea surface temperature (SST; Wu et al. 1999), and atmospheric ozone (Li et al. 2001). The 18 thermal spectral bands have approximately 10-km resolution. With GOES East and GOES West radiance measurements, atmospheric parameters can be monitored on an hourly basis over virtually all of the continental United States and large portions of adjacent oceanic regions. Cloud-top pressure and effective cloud amount are routinely generated using the $CO_2$-slicing technique (Schreiner et al. 2000, manuscript submitted to *J. Geophys. Res.*, hereinafter SSM) at the Cooperative Institute for Meteorological Satellite Studies, University of Wisconsin—Madison.

The accuracy of $CO_2$-slicing cloud-top height and the sources of errors have been investigated (Wielicki and Coakley 1981; Eyre and Menzel 1989; Wylie and Menzel 1989; Menzel et al. 1992; Schreiner et al. 1993; Baum and Wielicki 1994). Also, previous investigators have compared the $CO_2$-slicing cloud heights with those computed from lidar data (Smith and Platt 1978; Wylie and Menzel 1989; Smith and Frey 1990; Frey et al. 1999). Results show the $CO_2$-slicing heights are estimated to be within 50 hPa rms of other measurements. Comparisons between the $CO_2$-slicing and the pilot cloud reports also show that the $CO_2$-slicing assigned lower clouds than did pilot reports (SSM). However, because of the limited number of comparisons taken over a small geographical area, the validation for the $CO_2$-slicing cloud-top height is incomplete.

To use the information from all GOES longwave radiance measurements for the retrieval of cloud parameters, the 1DVAR scheme was applied to the GOES longwave spectral band cloudy radiances by assuming that the effective cloud amount (ECA) is independent of wavelength in the longwave $CO_2$ spectral region. The $CO_2$-slicing cloud parameters served as the background or the first-guess information required by the 1DVAR processing. This nonlinear algorithm simultaneously accounts for the instrument noise, the uncertainties of the radiative transfer model, the atmospheric temperature and moisture effects, and the satellite cloudy measurements. Because all longwave $CO_2$ spectral band cloudy radiances (a) are inversely weighted by their instrument noise along with the assumed forward model error and (b) are used simultaneously in the 1DVAR retrieval processing, noticeable improvements in 1DVAR cloud retrievals were found over the $CO_2$-slicing cloud parameters. The rmse of the $CO_2$-slicing-derived CTP would be expected to be reduced in 1DVAR. When very high clouds or low clouds exist and/or large satellite observation errors and uncertainties of radiative transfer model occur, the improvement should be even more significant. This 1DVAR approach was applied to process the *GOES-8* sounder spectral-band cloudy radiance measurements. The $CO_2$-slicing-derived CTPs were compared with the 1DVAR CTP retrievals in this paper.

Section 2 provides the formulation for calculating the GOES sounder longwave spectral-band cloudy radiances and formation of the $CO_2$-slicing algorithms. Section 3 describes the 1DVAR algorithm used for GOES CTP and ECA retrieval. Section 4 outlines the comparisons between the $CO_2$ slicing cloud parameters and 1DVAR cloud retrievals from simulated GOES sounder longwave spectral-band cloudy radiances. Section 5 investigates the effect of instrument noise on the 1DVAR improvement over the $CO_2$ slicing. Section 6 gives the comparisons between the $CO_2$-slicing and 1DVAR cloud retrievals from *GOES-8* sounder longwave spectral-band cloudy radiance measurements. The results and implications are discussed in section 7. Future extensions and conclusions are summarized in section 8.

## 2. GOES cloudy radiances and $CO_2$-slicing technique

If we neglect scattering by the atmosphere, the clear-sky radiance measured by GOES for a specific longwave infrared spectral band within a field-of-view (FOV) is given by

$$R_{\text{clr}} = \varepsilon_s B_s \tau_s - \int_0^{p_s} B \, d\tau(0, p) + (1 - \varepsilon_s) \int_0^{p_s} B \, d\tau^*, \quad (1)$$

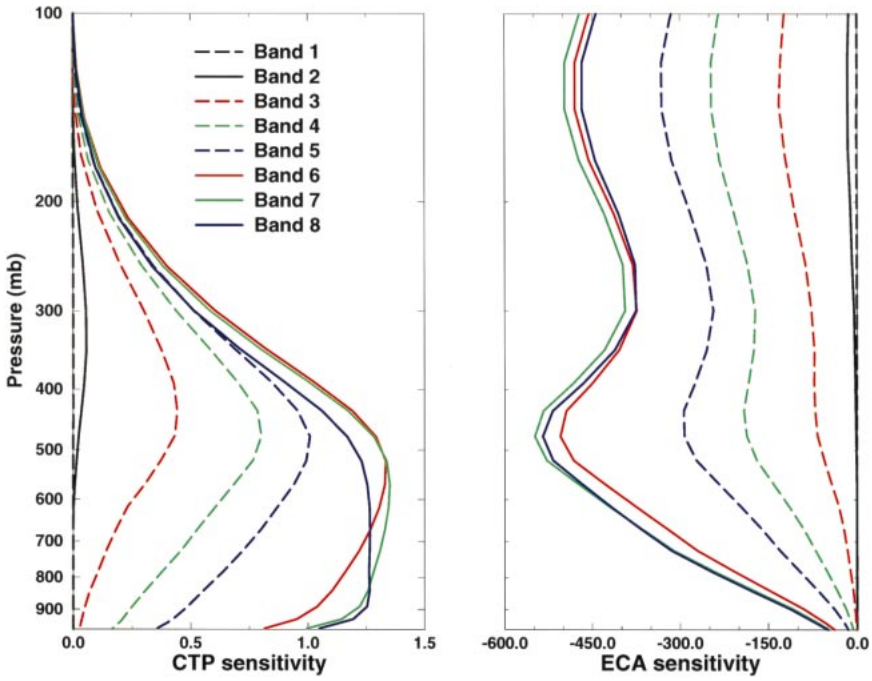


FIG. 1. The sensitivity functions for (left) an opaque (CTP) and (right) for ECA for the *GOES-8* spectral bands 1–8. The sensitivities for CTP and ECA are defined as $\partial R/\partial p_c$ and $\partial R/\partial(N\varepsilon_c)$, respectively, and are scaled by $d\ \ln p$. The *U.S. Standard Atmosphere, 1976*, was used in the transmittance calculations for this figure.

where $R_{\rm clr}$ is the clear spectral radiance in the infrared region, as seen by the satellite sensor; $B$ is the Planck radiance, which is a function of pressure $p$; $\tau$ is the atmospheric transmittance function; subscript $s$ denotes surface; $\tau^* = \tau_s^2/\tau$; and $\varepsilon_s$ is the surface emissivity. For an overcast black ($\varepsilon_c = 1$) cloud at pressure $p_c$, the radiance $R_{\rm cld}$ is given by

$$R_{\rm cld} = B_c\tau_c - \int_0^{p_c} B\, d\tau(0, p), \qquad (2)$$

where subscript $c$ denotes the cloud top. The upwelling radiance $R$ for a partially cloud-filled FOV is given by

$$R = (1 - N\varepsilon_c)R_{\rm clr} + N\varepsilon_c R_{\rm cld}, \qquad (3)$$

where the cloud emissivity $\varepsilon_c$ is multiplied by the cloud fractional coverage $N$ and the quantity $N\varepsilon_c$ is referred to as the effective cloud amount.

To determine the retrieval accuracy, a precise knowledge of the instrument performance and the accuracy of the atmospheric transmittance functions for the various spectral bands is crucial. In this paper, a fast and accurate transmittance model called pressure-layer optical depth or pressure-layer fast algorithm for atmospheric transmittances (Hannon et al. 1996) is used; it has 42 pressure-level vertical coordinates from 0.1 to 1050 hPa. The calculations take into account the satellite zenith angle, absorption by well-mixed gases (including nitrogen, oxygen, and carbon dioxide), water vapor (including the water vapor continuum), and ozone. To analyze the cloud information observed by the GOES longwave spectral bands, a linearized differential form of Eq. (3) with respect to CTP and ECA is obtained (see appendix):

$$\delta R = (R_{\rm cld} - R_{\rm clr})\delta(N\varepsilon_c) + (N\varepsilon_c)\tau_c\frac{\partial B_c}{\partial p_c}\delta p_c. \qquad (4)$$

Thus $\partial R/\partial(N\varepsilon_c) = R_{\rm cld} - R_{\rm clr}$, and $\partial R/\partial p_c = (N\varepsilon_c)\tau_c(\partial B_c/\partial p_c)$, where $\partial R/\partial(N\varepsilon_c)$ and $\partial R/\partial p_c$ are the sensitivity functions of ECA and CTP. Figure 1 shows the sensitivity functions for an opaque CTP (left panel of the figure) and for ECA (right panel of the figure) of the *GOES-8* longwave spectral bands 1–8; the *U.S. Standard Atmosphere, 1976*, was used in the transmittance calculations for this figure. Note that the actual sensitivity to CTP should be the magnitude in this figure times ECA; therefore, thick clouds have more sensitivity for the CTP than thin clouds. Usually, band 1 provides almost no information for clouds, because it is an upper-stratospheric band; band 2 provides some sensitivity to very high clouds; and bands 3–8 are sensitive to cloud. Figure 2 shows the *GOES-8* longwave spectral-band images at 2346 UTC 6 October 1999. The CTP information is limited to approximately 200 hPa. The reason for the limitation is physical; a close inspection of the GOES radiance weighting functions ($d\tau/d\ \ln p$) (Menzel et al. 1998) for the four longwave $CO_2$ absorption bands used to determine CTP reveals that they all peak between 200 hPa and the surface. All spectral bands have

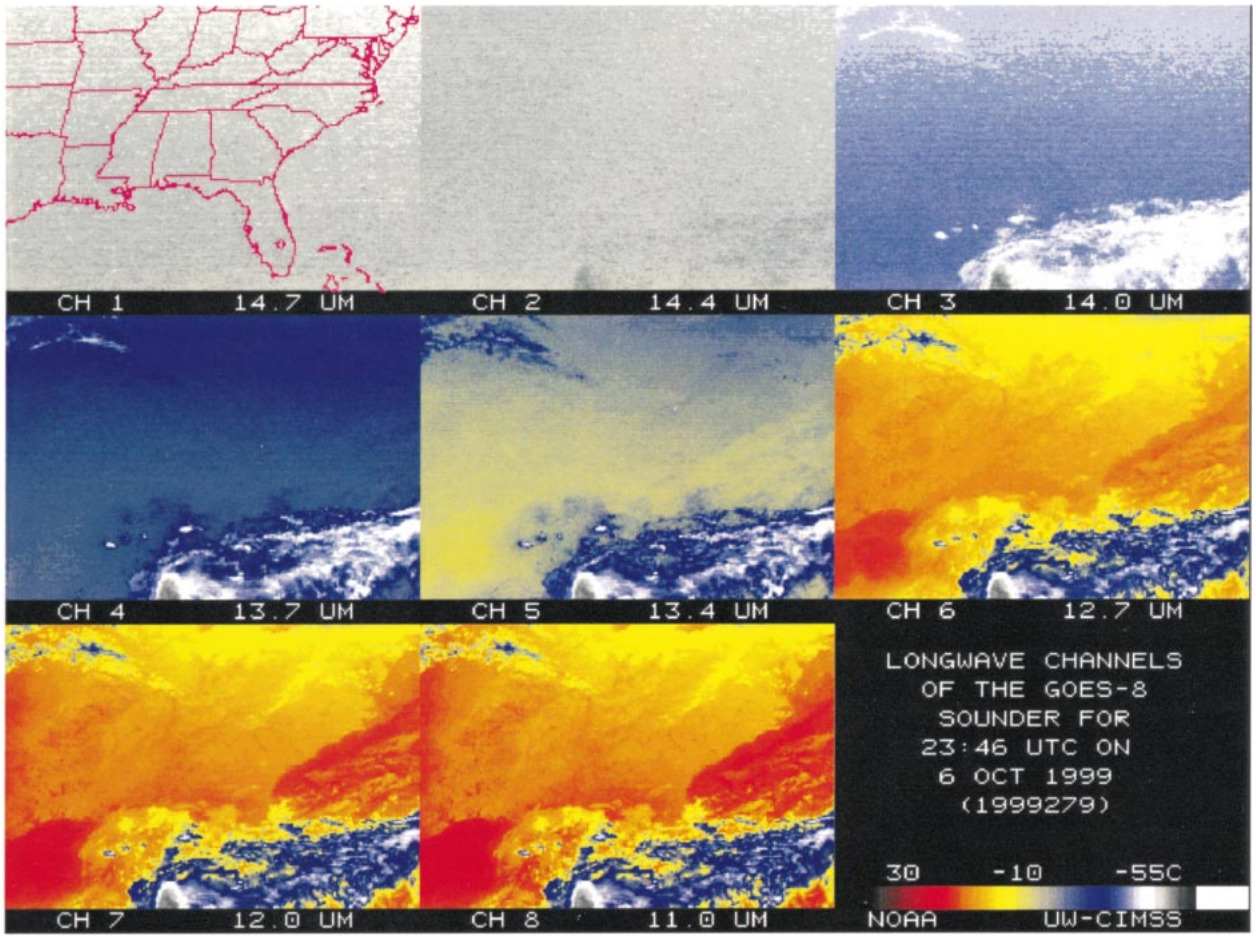


FIG. 2. The *GOES-8* longwave spectral-band (bands 1–8) images at 2346 UTC 6 Oct 1999. Cloud signal still can be seen on the band-2 image.

the maximum cloud-top sensitivities at approximately 450–500 hPa, and bands 6–8 have some sensitivity at lower levels. For ECA, all the bands have sensitivities for most pressure levels above 700 hPa; this result is due to the fact that the ECA sensitivity is the difference between clear and overcast radiances $[\partial R/\partial(N\varepsilon_c) = R_{\rm cld}(p_c) - R_{\rm clr}]$, and the difference is significantly large with a CTP ($p_c$) above 700 hPa. For low clouds ($p_c \rightarrow p_s$), because the difference between clear and overcast radiances is small $[R_{\rm cld}(p_c) \rightarrow R_{\rm clr}]$, the sensitivity is limited, as indicated by Fig. 1.

As described by Menzel et al. (1992), the basic assumptions of the $CO_2$-slicing algorithm are as follows: (a) the emissivity of the cloud is the same in the $CO_2$ spectral-band pairs, and the $CO_2$ radiances sense the same region of cloud; (b) clouds occur as a single thin layer; and (c) the surface temperature and the temperature structure of the atmosphere, as well as its transmittance at the $CO_2$ wavelengths, are known. The working equation was previously discussed in Wylie and Menzel (1989). To assign a CTP to a given cloud, the ratio of the deviations in cloud-produced radiances and the corresponding clear sky radiances for two spectral bands $\nu_1$ and $\nu_2$ viewing the same FOV are written as

$$\frac{R(\nu_1) - R_{\rm clr}(\nu_1)}{R(\nu_2) - R_{\rm clr}(\nu_2)} = \frac{N\varepsilon_{c1}\left\{\int_{p_s}^{p_c} \tau_1\, dB_1 + (1-\varepsilon_{s1})\left[B_1(0)\tau_{s1}^2 - \int_{p_s}^{0} \tau_1^*\, dB_1\right]\right\}}{N\varepsilon_{c2}\left\{\int_{p_s}^{p_c} \tau_2\, dB_2 + (1-\varepsilon_{s2})\left[B_2(0)\tau_{s2}^2 - \int_{p_s}^{0} \tau_2^*\, dB_2\right]\right\}}. \quad (5)$$

The cloudy radiances in Eq. (5), $R(\nu_1)$ and $R(\nu_2)$, are the measured satellite data and clear radiances for a cloudy FOV; $R_{\rm clr}(\nu_1)$ and $R_{\rm clr}(\nu_2)$ are retrieved from the neighboring clear FOVs or calculated from the background profile information. The radiative transfer calculations implicit on the right side of Eq. (5) are performed using the radiative properties of the atmosphere in the $CO_2$ spectral bands given a background temper-

ature profile. The only variables in Eq. (5) are CTP and ECA. Because ECA is assumed to be constant for the two spectral bands, CTP can be calculated by minimizing the difference between the two sides of Eq. (5). Also, ECA can be calculated from the infrared window (band 8) using the $CO_2$-slicing CTP. Using Eq. (3), one can write

$$N\varepsilon_c = \frac{R - R_{\text{clr}}}{R_{\text{cld}} - R_{\text{clr}}}. \tag{6}$$

If no ratio of radiances can be reliably calculated in Eq. (5), because $(R_{\text{clr}} - R)$ is too small and hence within the instrument noise level, then the cloud is assumed to be opaque, and a CTP is calculated directly from the infrared window channel radiance observations and the background temperature profile. Simulation study shows that changing the noise threshold will affect the percentage of heights assigned by $CO_2$ versus IR window, especially for low clouds. The effect for most medium and high clouds (ECA $>$ 0.3) is small because of the large contrast between clear calculation and observation except for very thin clouds (ECA $<$ 0.3) that are likely to be determined to be clear. If the threshold is reduced by one-half, the cases assigned to the IR window technique are reduced by approximately 10% for most low clouds (ECA $>$ 0.3); if the threshold is doubled, the cases assigned to the IR window technique are increased by approximately 15% for most low clouds (ECA $>$ 0.3). Note that the ECA retrieval in the IR window technique is always 1.0. Hereinafter, the $CO_2$-slicing algorithm refers generally to the radiance ratio method in Eq. (5) as well as to the window technique.

## 3. The physical inversion scheme

By making the same assumptions adopted by the $CO_2$-slicing algorithm described in section 2, the 1DVAR method uses the $CO_2$-slicing-derived CTP and ECA as the background or the first guess to calculate the nonlinear optimal solution of cloud parameters from the GOES longwave spectral-band cloudy radiance measurements. If the GOES observed cloudy radiance $R$ for each spectral band is known, then $R$ can be considered a nonlinear function of the atmospheric temperature profile, water vapor mixing ratio profile, surface skin temperature, surface emissivity, CTP, and ECA. That is, $R = R(T, q, T_s, \varepsilon_s, p_c, N\varepsilon_c)$, or, in general, for all spectral bands,

$$\mathbf{Y} = F(\mathbf{X}), \tag{7}$$

where the vector $\mathbf{X}$ contains CTP and ECA (the atmospheric temperature profile, moisture profile, surface skin temperature, and IR surface emissivity are assumed to be known or obtained from the forecast analysis), and $\mathbf{Y}$ contains $N$ satellite-observed cloudy radiances. The linear form of Eq. (7) is

$$\delta\mathbf{Y} = F'\,\delta\mathbf{X}, \tag{8}$$

where $F'$ is the linear or tangent model of the forward model $F$, which is outlined by Eq. (4).

The general idea of the 1DVAR theory is to minimize a penalty function $J(\mathbf{X})$, which measures the degree of fit of the cloudy measurements to the background information and possibly to other physical constraints. A general form of the 1DVAR solution is to minimize the following penalty function (Rodgers 1976):

$$J(\mathbf{X}) = [\mathbf{Y}^m - \mathbf{Y}(\mathbf{X})]^{\mathrm{T}}\mathbf{E}^{-1}[\mathbf{Y}^m - \mathbf{Y}(\mathbf{X})] + [\mathbf{X} - \mathbf{X}_0]^{\mathrm{T}}\mathbf{B}^{-1}[\mathbf{X} - \mathbf{X}_0], \tag{9}$$

where the vector $\mathbf{X}$ contains the CTP and ECA that need to be solved; $\mathbf{X}_0$ is the background or the first guess of $\mathbf{X}$, where $\mathbf{X}_0$ is obtained from the $CO_2$-slicing technique; $\mathbf{Y}^m$ is the vector of the observed cloudy radiances used in the retrieval process in which a total of eight longwave spectral bands were used (note that band 1 provides no cloud information); $\mathbf{Y}(\mathbf{X})$ is a vector of cloudy radiances calculated from the cloud state $\mathbf{X}$; $\mathbf{E}$ is the observation error covariance matrix, which includes instrument noise plus the assumed forward model error; $\mathbf{B}$ is the assumed background error covariance matrix, which constrains the solution; and the superscript T denotes the transpose.

The solution $\mathbf{X}$ minimizes the penalty function. Figure 3 depicts the penalty function with respect to CTP and ECA for a CTP of 500 hPa and an ECA of 0.5; the *GOES-8* spectral-band cloudy radiances were simulated with nominal *GOES-8* instrument noise plus 0.2 K forward model error for each spectral band. The background cloud parameters from the $CO_2$ slicing were assumed to be 350 hPa for CTP and 0.36 for ECA in this figure. In Eq. (9), the solution $\mathbf{X}$ could be considered as a modification of the background $\mathbf{X}_0$. The two terms reflect the weighted satellite measurement and background contributions to the solution, respectively. In the penalty function, if the variable $\mathbf{X}$ is either a small modification of the background $\mathbf{X}_0$ $\{\mathbf{X} \to \mathbf{X}_0, J(\mathbf{X}) \to [\mathbf{Y}^m - \mathbf{Y}(\mathbf{X}_0)]\mathbf{E}^{-1}[\mathbf{Y}^m - \mathbf{Y}(\mathbf{X}_0)]\}$ or a large deviation from the background $\mathbf{X}_0$, then $J(\mathbf{X})$ might not reach the minimum (Li and Huang 1999). In Fig. 3, the solution $\mathbf{X}$ (492 hPa for CTP and 0.476 for ECA) that makes $J(\mathbf{X})$ a minimum can be regarded as a proper modification of the background $\mathbf{X}_0$ (350 hPa for CTP and 0.36 for ECA from the $CO_2$ slicing). To solve Eq. (9), the following Newtonian iteration is used:

$$\mathbf{X}_{n+1} = \mathbf{X}_n + J''(\mathbf{X}_n)^{-1} \cdot J'(\mathbf{X}_n), \tag{10}$$

and the following quasi-nonlinear iterative form (Eyre 1989) is obtained:

$$\delta X_{n+1} = (F_n'^{\mathrm{T}}\mathbf{E}^{-1}F_n' + \mathbf{B}^{-1})^{-1}F_n'^{\mathrm{T}}\mathbf{E}^{-1}(\delta\mathbf{Y}_n + F_n'\delta\mathbf{X}_n), \tag{11}$$

where $\delta\mathbf{X}_n = \mathbf{X}_n - \mathbf{X}_0$, $\delta\mathbf{Y}_n = \mathbf{Y}^m - \mathbf{Y}(\mathbf{X}_n)$, and $F_n'$ from Eq. (8) represents the linear terms with $\delta R$ expansion of Eq. (4).

In the GOES data processing, the $CO_2$-slicing-derived CTP and ECA serve as the cloud background in the

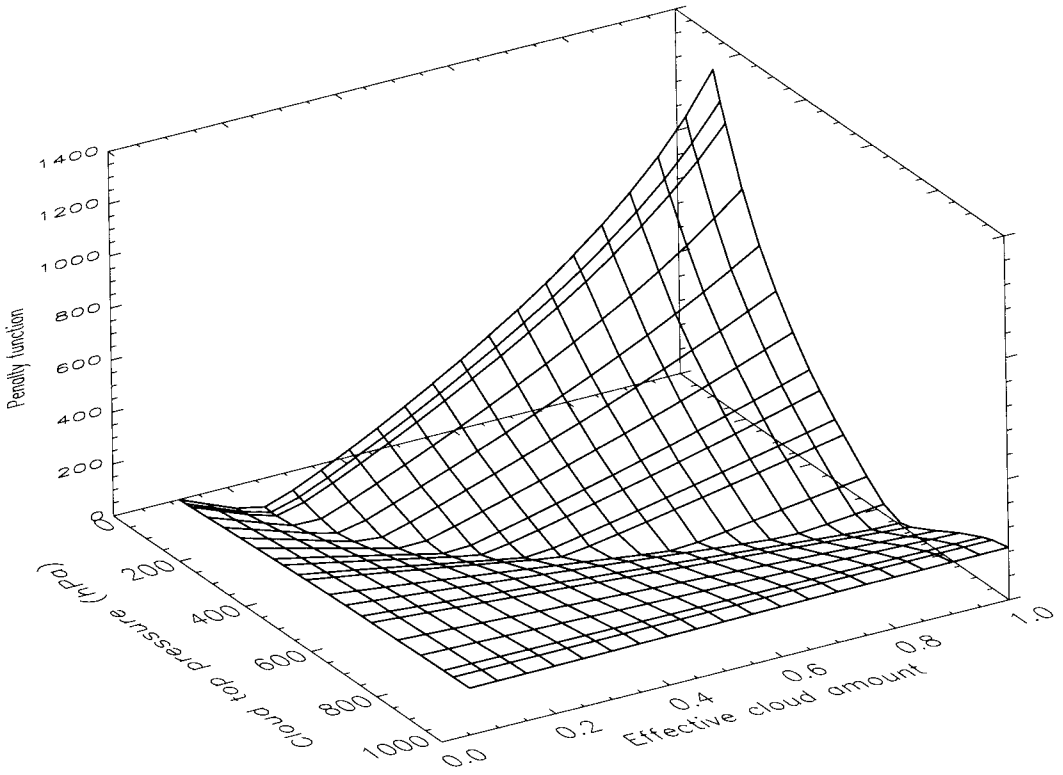


FIG. 3. The penalty function with respect to CTP and ECA for a CTP of 500 hPa and an ECA of 0.5; the *GOES-8* spectral-band cloudy radiances were simulated with nominal *GOES-8* instrument noise plus 0.2 K forward model error. The background cloud parameters from $CO_2$ slicing are assumed to be 350 hPa for CTP and 0.36 for ECA.

1DVAR retrieval processing. Hourly surface temperature observations from the National Weather Service (NWS) or the forecast analysis are used as the surface skin temperature. Temperature and moisture profiles were obtained from the National Centers for Environmental Prediction (NCEP) forecast analysis. Menzel et al. (1998) investigated the temperature sounding information from the GOES sounder spectral-band radiance measurements. Statistically, there are only slight changes of the GOES temperature sounding over the forecast first guess under clear-sky conditions, suggesting that the GOES sounder radiances rarely provide additional temperature sounding information beyond the forecast analysis over the continental United States.

The background error covariance matrix $\mathbf{B}$ is assumed to be diagonal, with a standard deviation (square root of the diagonal element) of 100 hPa for the CTP error and 0.15 for ECA. Rather than using CTP, the logarithm of CTP is used to stabilize the solution of Eq. (9). Therefore, the background error for $\ln p_c$ should be $\Delta \ln p_c = \Delta p_c / p_c$; assuming that the averaged CTP is 500 hPa, the background error for the logarithm of the CTP is 0.04. If the background covariance matrix is not known, other constraints can be applied to solve Eq. (9); for example, using a smoothing factor $\gamma$ instead of inverse of the background error covariance matrix $\mathbf{B}^{-1}$ in the penalty function; the smoothing factor can be determined empirically (Susskind et al. 1984; Smith et al. 1985; Hayden 1988) or by the discrepancy principle (Li and Huang 1999; Li et al. 2000). The cloudy radiance vector $\mathbf{Y}^m$ is obtained from the GOES longwave spectral bands 1–8. The measurement error covariance matrix $\mathbf{E}$ is a fixed diagonal matrix. Each diagonal element is the square of the GOES instrument noise (see Table 1) plus an assumed forward model error of 0.2 K for each longwave spectral band.

## 4. Cloud retrievals from simulated GOES longwave cloudy radiances

To compare the $CO_2$-slicing and 1DVAR cloud parameter retrievals, a simulation study was conducted. A set of 1336 global radiosonde profiles, which represent various atmospheric conditions coincident with the GOES sounder geographical coverage, were selected for this simulation. Forty combinations were formed from each profile by assigning four CTPs plus 50-hPa random variation (200, 300, 550, and 850 hPa corresponding to very high, high-, medium-, and low-level clouds) and 10 ECAs (0.1, 0.2, 0.3, 0.4, 0.5, 0.6, 0.7, 0.8, 0.9, and 1.0). The *GOES-8* longwave spectral-band cloudy radiances were simulated for all combinations of each profile. An IR surface emissivity of 0.98 for each longwave spectral band was assumed in the simulation. The

TABLE 1. *GOES-8* longwave sounder noise performance. NEDR is the in-flight measured noise equivalent radiation (mW $m^{-2}$ $sr^{-1}$ $cm^{-1}$); spec is the prelaunch specific value.

| Wavelength ($\mu$m) | Band | NEDR (mW $m^{-2}$ $sr^{-1}$ $cm^{-1}$) | Spec |
|---|---|---|---|
| 14.7 | 1 | 1.63 | 0.66 |
| 14.4 | 2 | 1.41 | 0.58 |
| 14.1 | 3 | 0.94 | 0.54 |
| 13.9 | 4 | 0.65 | 0.45 |
| 13.4 | 5 | 0.74 | 0.44 |
| 12.7 | 6 | 0.32 | 0.25 |
| 12.0 | 7 | 0.21 | 0.16 |
| 11.0 | 8 | 0.15 | 0.16 |

nominal *GOES-8* instrument noise listed in Table 1 plus an assumed forward model error of 0.2 K were added into each *GOES-8* spectral-band cloudy radiance. Cloud retrievals from both $CO_2$ slicing and 1DVAR were obtained from those simulated *GOES-8* spectral-band cloudy radiances.

To account for the surface uncertainties and the atmospheric profile error in the cloud retrievals, nominal errors were considered in the simulation. For atmospheric temperature, a 2.0 K random error was assumed at each pressure level, which is close to the accuracy of the forecast analysis. The surface skin temperature has a large effect on the IR window radiances, and the background surface skin temperature from an hourly surface temperature observation or the forecast analysis usually has a large error. For surface skin temperature, a nominal random error of 2.5 K was assumed in the simulation. In addition, 1.0% error was included for IR surface emissivity, and 15% error was included for water vapor mixing ratio at each pressure level. It should be noted that 1) when a cloudy case is declared clear (it usually happens for low clouds or very thin high and medium clouds), a CTP of 1000 hPa and an ECA of zero are assigned for the statistics; 2) when 1DVAR fails because of iterative divergence, the 1DVAR retrieval is set to the $CO_2$ slicing cloud parameters.

The cloud retrievals are compared with the true cloud parameters. Figure 4 shows the retrieved bias (''true''

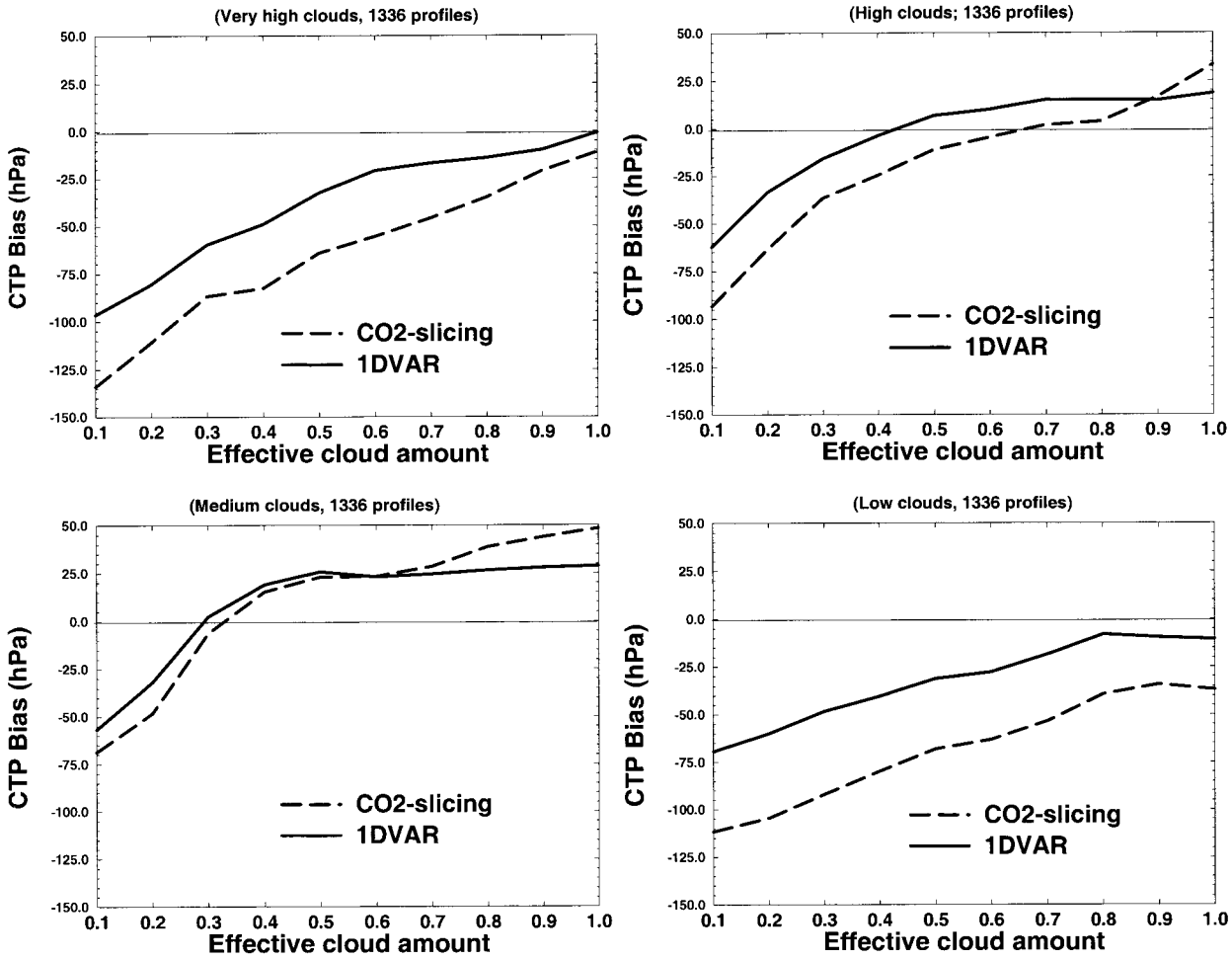


FIG. 4. The retrieved bias (true minus retrieval) for CTP using the $CO_2$-slicing and 1DVAR algorithms for the four different cloud types (very high, high, medium, and low clouds).

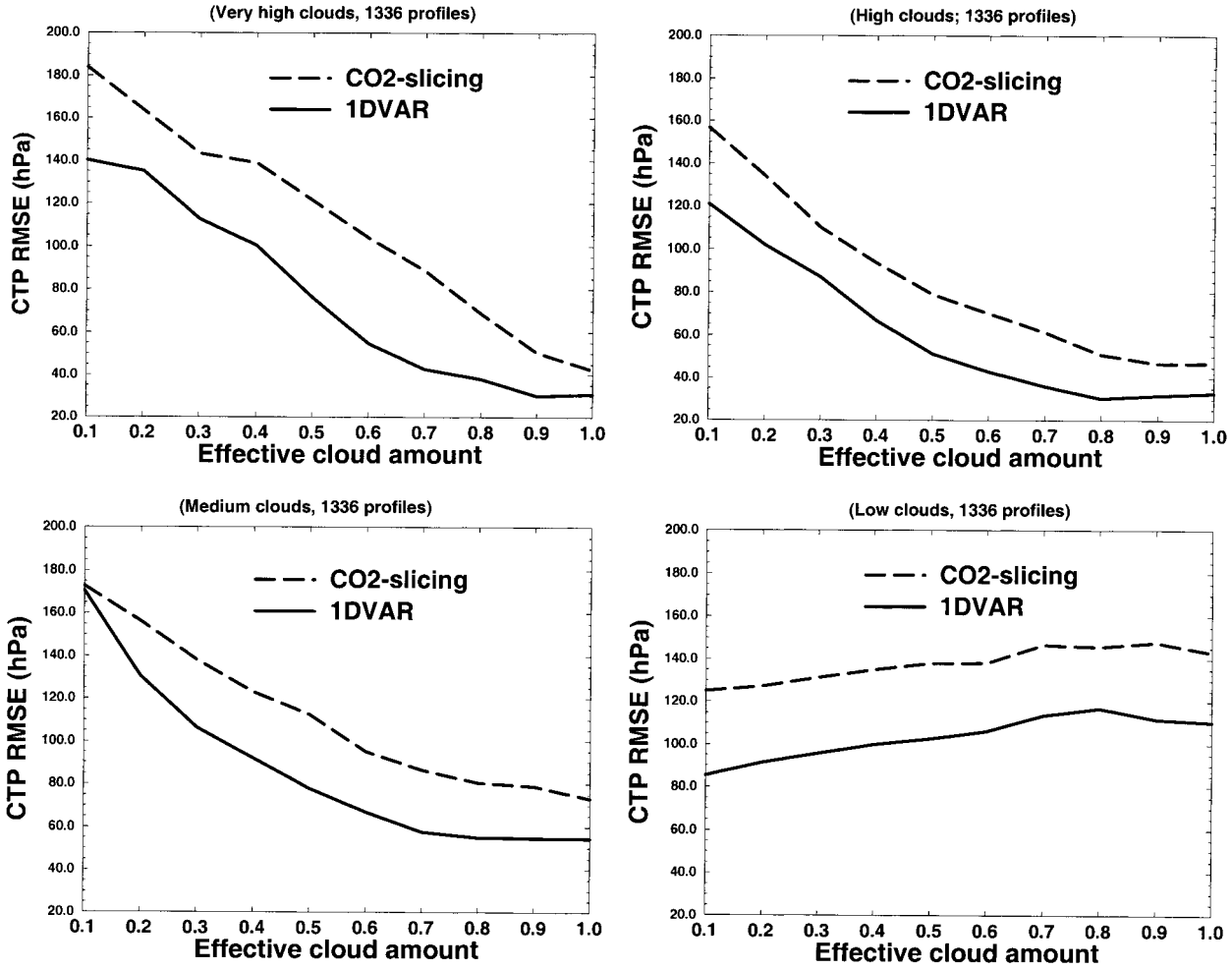


FIG. 5. The retrieved rmse for CTP using the $CO_2$-slicing and 1DVAR algorithms for the four different cloud types (very high, high, medium, and low clouds).

minus retrieval) for the CTP using the $CO_2$-slicing and 1DVAR algorithms for the four cloud types. For very high cloud (upper-left panel), the $CO_2$ slicing can have a bias as large as 130 hPa for thin cirrus clouds, ECA less than 0.5. This result is due to the fact that the GOES spectral band pair used in the $CO_2$-slicing technique has limited cloud-top information for very high clouds. Usually, the $CO_2$ slicing assigned clouds to lower levels. The 1DVAR reduced the $CO_2$-slicing bias by 10–40 hPa, but 1DVAR still has a bias for the thin, very high clouds. For high clouds (upper right), the $CO_2$ slicing produced a relatively large bias for very thin clouds, ECA less than 0.3; 1DVAR reduced this bias by 20–30 hPa. Both $CO_2$ slicing and 1DVAR performed well for most thick high clouds, ECA greater than 0.5. For medium clouds (lower left), $CO_2$ slicing and 1DVAR are similar, but 1DVAR does show a slight improvement for most medium clouds. An improvement of 10–20 hPa is seen in 1DVAR over $CO_2$ slicing for very thick clouds, ECA greater than 0.8. For low clouds (lower right), $CO_2$ slicing has a large bias, because only the window band is used to estimate the cloud-top pressure. By using all the longwave spectral bands (see Fig. 1), 1DVAR is able to reduce the low bias of the $CO_2$ slicing in low cloud retrievals by 25–50 hPa.

The rmse was calculated with Eq. (12) to illustrate the performance of $CO_2$ slicing and 1DVAR:

$$\text{rmse} = \left[\frac{1}{\text{NS}}\sum_{j=1}^{\text{NS}}(X_j^{\text{true}} - X_j^{\text{rtvl}})^2\right]^{1/2}, \qquad (12)$$

where $X_j^{\text{true}}$ and $X_j^{\text{rtvl}}$ are the truth and retrieval for the $j$th sample, respectively, and NS is the total number of samples. Figure 5 shows the retrieved rmse for CTP using the $CO_2$-slicing and 1DVAR algorithms for the four cloud types. The 1DVAR significantly reduced the rmse by 10–50 hPa for most of the very high clouds (upper left) and the high clouds (upper right). These improvements are mainly due to the reduction of bias in 1DVAR over the $CO_2$ slicing. For medium clouds (lower left), an improvement of 10–35 hPa in rmse is found in 1DVAR over the $CO_2$ slicing. For low clouds

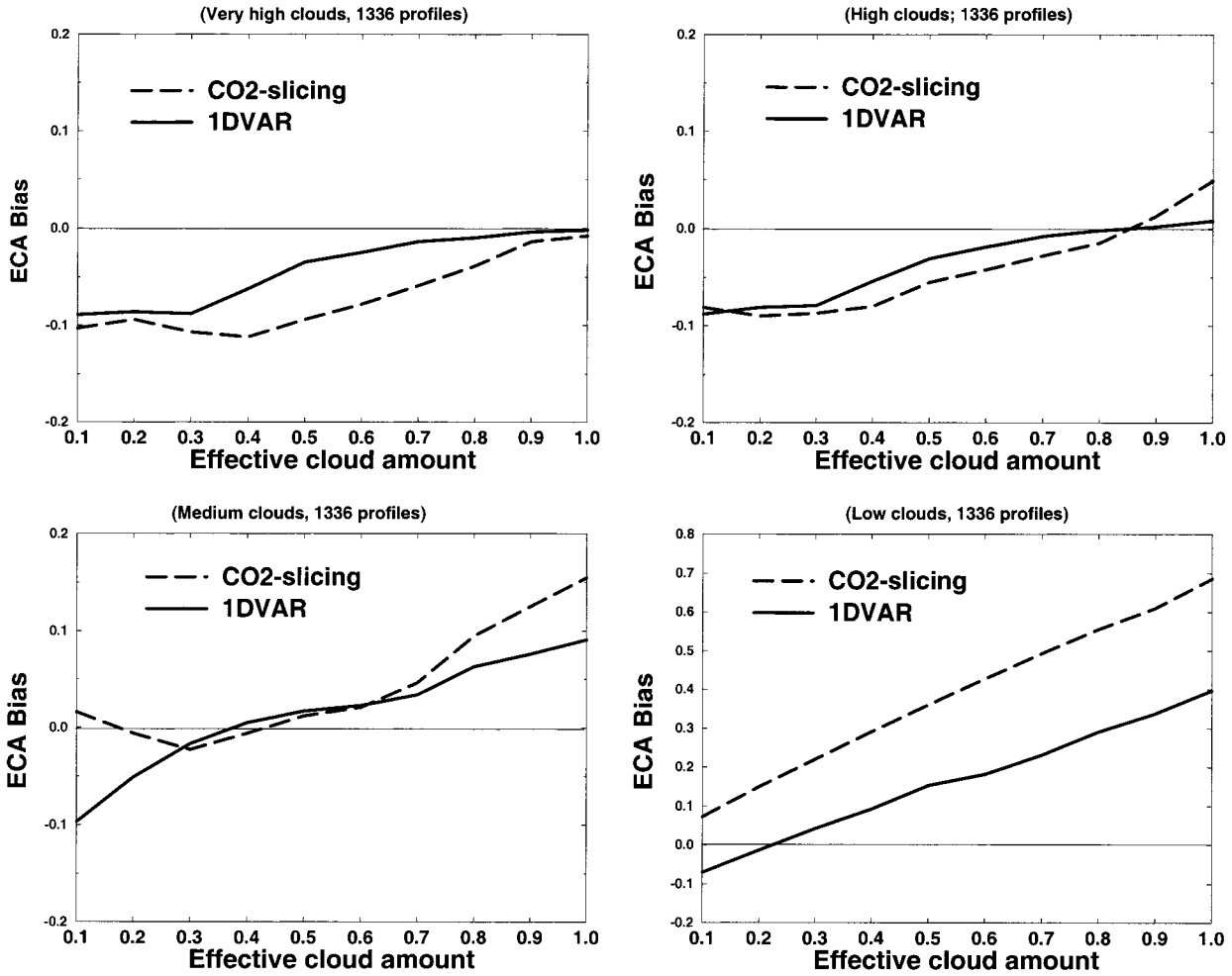


FIG. 6. The retrieved bias (true minus retrieval) for ECA using the $CO_2$-slicing and 1DVAR algorithms for the four different cloud types (very high, high, medium, and low clouds).

(lower right), the rmse is reduced by approximately 35 hPa. Again, this improvement results from the bias reduction in 1DVAR over the $CO_2$-slicing method.

Figure 6 shows the retrieved bias (''true'' minus retrieval) for the ECA using the $CO_2$-slicing and 1DVAR algorithms for the four cloud types. A significant improvement of 0.1–0.3 is found in 1DVAR over $CO_2$ slicing for low clouds. Slight improvement is also seen for very high, high, and medium clouds. 1DVAR is worse for very thin medium clouds (ECA $< 0.3$); it is not clear what causes this result in this simulation study. Figure 7 shows the retrieved rmse for ECA using the $CO_2$-slicing and 1DVAR algorithms for the four cloud types. A systematic improvement of 1DVAR over the $CO_2$ slicing is found for all types of clouds. An improvement of 0.1–0.2 is found for thick low clouds, ECA greater than 0.5.

It is interesting that rmse of ECA decreases from thin to thick for high clouds, while it increases for low clouds. Eyre and Menzel (1989) observed similar results for low clouds. The cause for this can be revealed by an additional error analysis of ECA with respect to CTP. Using Eqs. (6) and (A7), one can write

$$\Delta(N\varepsilon_c) = -\frac{\tau_c\left(\frac{\partial B_c}{\partial p_c}\right)}{R_{\text{cld}} - R_{\text{clr}}}(N\varepsilon_c)\Delta p_c. \qquad (13)$$

For high and medium clouds, $\Delta p_c$ significantly increases with decreasing $N\varepsilon_c$ (see Fig. 5) and $R_{\text{cld}} - R_{\text{clr}}$ has large absolute value. Therefore, the error of ECA may be large for thin clouds. However, for low clouds, because the CTP error $\Delta p_c$ is relatively constant for different ECAs and $R_{\text{cld}} - R_{\text{clr}}$ is small, the error of ECA may increase as $N\varepsilon_c$ increases.

The results presented so far contain some cloudy situations that are determined to be clear by the retrieval processing; for example, some thin high- and midcloud cases sometimes are determined to be clear. In addition, most low-cloud cases are processed by the window technique. To evaluate the performance of pure $CO_2$ slicing

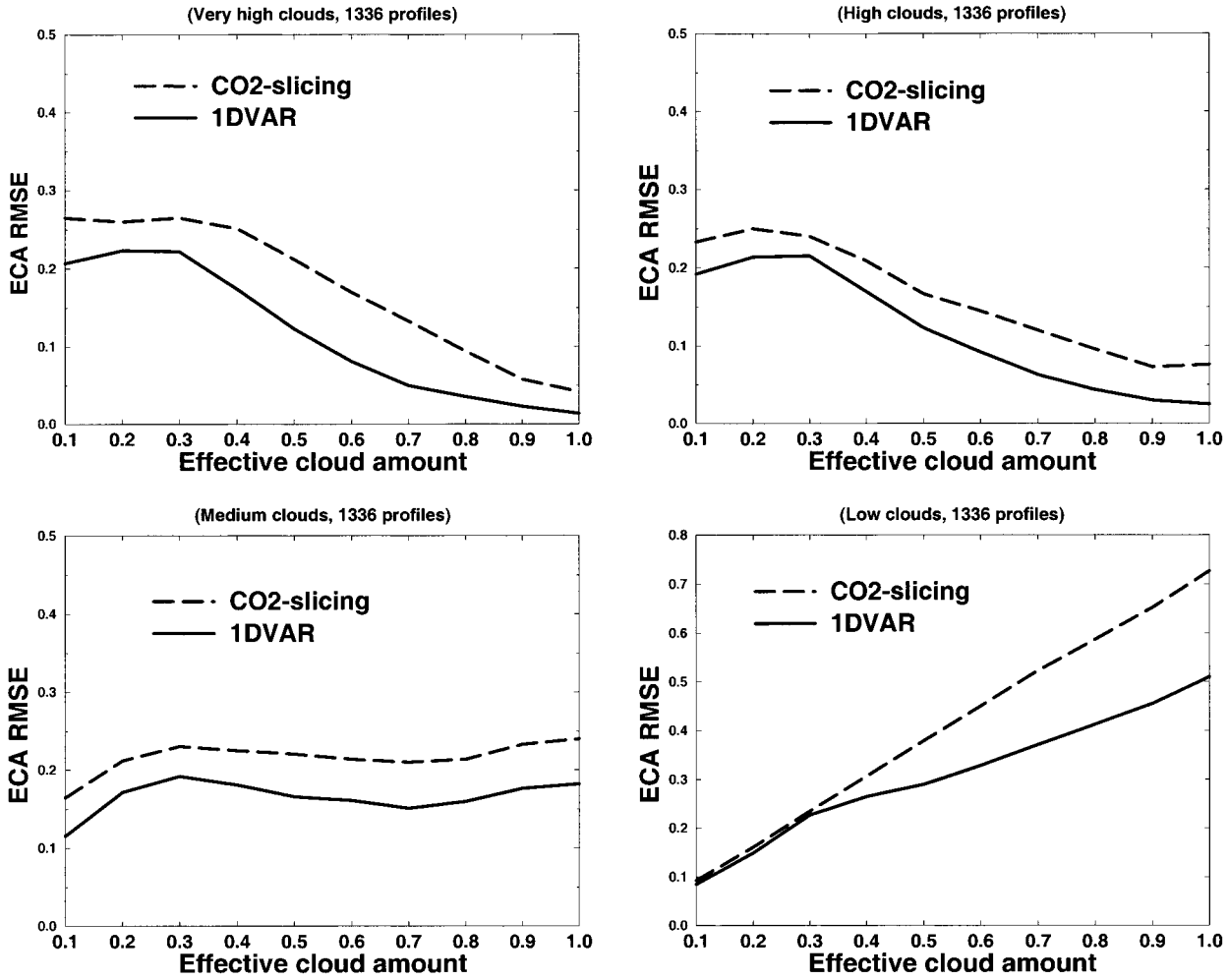


FIG. 7. The retrieved rmse for ECA using the $CO_2$-slicing and 1DVAR algorithms for the four different cloud types (very high, high, medium, and low clouds).

(without window technique) followed by 1DVAR, the cases with only pure $CO_2$ slicing were selected in the result statistics. Because of the fact that there are very few pure $CO_2$-slicing cases for low clouds, only very high, high-, and medium-cloud cases are reevaluated. Figure 8 shows the retrieved rmse for the CTP from pure $CO_2$ slicing followed by 1DVAR algorithms for very high, high-, and medium-cloud types. The percentage of pure $CO_2$-slicing cases (shown at the lower-right panel) indicates that $CO_2$ slicing performs successfully for most high and medium clouds except for very thin medium clouds (ECA $< 0.3$). Because $R - R_{\text{clr}} = (N\varepsilon_c)(R_{\text{cld}} - R_{\text{clr}})$ is used in the $CO_2$ slicing, thin clouds $[(N\varepsilon_c) \rightarrow 0]$ or low clouds $[(R_{\text{cld}} - R_{\text{clr}}) \rightarrow 0]$ might be determined to be clear. Of course, a thin medium cloud is more likely to be determined to be clear than a thin high cloud. For thick very high, high, and medium clouds (ECA $> 0.5$), only few cases are determined with the window technique. The rmse of pure $CO_2$ slicing is reduced somewhat for very thin clouds as compared with Fig 5. Still, 1DVAR significantly reduced the rmse by 10–50 hPa for most of the very high clouds (upper left) and high clouds (upper right). For medium clouds (lower left), an improvement of 20–35 hPa in rmse is found in 1DVAR over the pure $CO_2$ slicing.

Note that the rmse accuracy of the $CO_2$-slicing technique for this simulation with 1336 profiles distributed globally may be somewhat different from those with only climate mean profiles (Wielicki and Coakley 1981; Baum and Wielicki 1994). The $CO_2$-slicing results, however, are close to those of Eyre and Menzel (1988), who used 200 profiles in their simulation.

## 5. Effect of GOES instrument noise on 1DVAR improvement over the $CO_2$ slicing

Menzel et al. (1992) investigated errors from instrument noise and uncertainties in temperature and moisture profiles in the $CO_2$-slicing algorithm. They con-

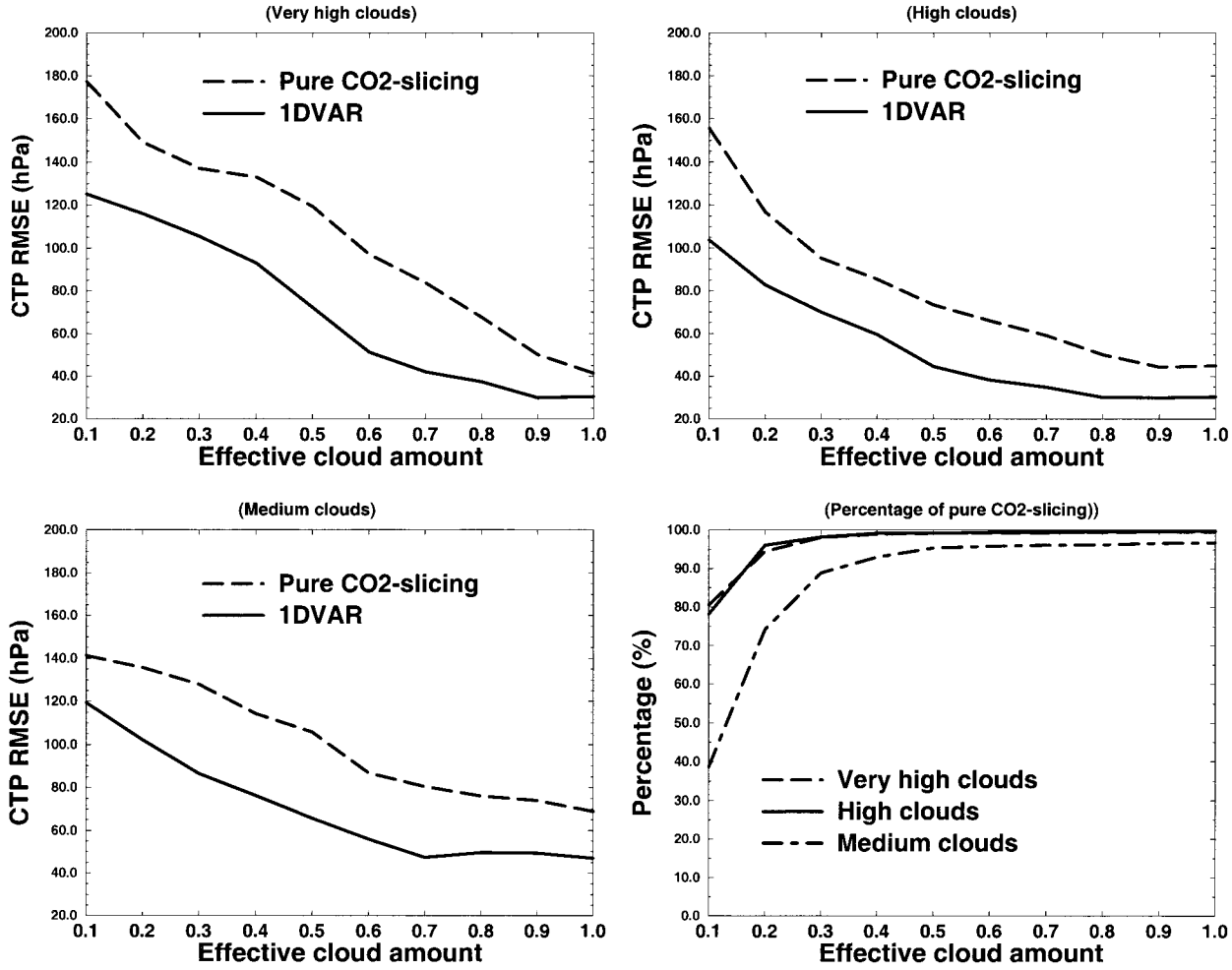


FIG. 8. The retrieved rmse for CTP from the pure $CO_2$-slicing followed by 1DVAR algorithms for very high, high, and medium cloud types. The percentages of pure $CO_2$-slicing cases are also shown at the lower-right panel.

cluded that errors from the $CO_2$-slicing-retrieved CTP resulting from inaccurate atmospheric temperatures should not be large. However, the $CO_2$ slicing may be sensitive to the instrument noise, because a ratio of radiance differences is used in the $CO_2$-slicing algorithm. In this paper, a simulation study was also carried out to account for the effect of GOES instrument noise on the 1DVAR improvement over the $CO_2$ slicing.

Hereinafter, the simulation with nominal instrument noise and nominal surface and atmospheric errors is defined as the nominal simulation. To investigate the influence of the instrument noise on the 1DVAR improvement over the $CO_2$ slicing, additional simulations were carried out with the *GOES-8* nominal instrument noise adjusted by a noise factor NF. The NF was set to 0.5 (low noise), 1.0 (nominal noise as described above), and 1.5 (high noise), respectively, in the simulation. The retrieval results for NF = 1.0 are exactly the same as those shown in the nominal simulation (Figs. 4–7). Figure 9 shows the rmse differences (RMSE-DIFF) between $CO_2$ slicing and 1DVAR (rmse of $CO_2$ slicing minus rmse of 1DVAR) for CTP with three different instrument noise factors (0.5, 1.0, and 1.5). A positive RMSE-DIFF indicates an improvement of the 1DVAR retrieval over $CO_2$ slicing, and a negative RMSE-DIFF means a degradation. For thin, very high and high clouds (ECA $<$ 0.5), the improvement of the 1DVAR technique is dependent on the instrument noise. High instrument noise (NF = 1.5) results in large improvement (40–50 hPa), and low instrument noise (NF = 0.5) gives less improvement (20–45 hPa) for very high clouds (upper-left panel). For high clouds (upper-right panel), high instrument noise (NF = 1.5) results in an improvement of 30–45 hPa, and low instrument noise (NF = 0.5) gives an improvement of only 15–20 hPa. This result means the $CO_2$-slicing error for thin, high clouds is amplified by the large instrument noise, but 1DVAR is able to reduce this amplified error. However, for the thick, high clouds (ECA $>$ 0.5), the instrument noise has only a slight influence on the 1DVAR improvement over the $CO_2$ slicing. This result might be due to the fact that the contrast between the observed and clear

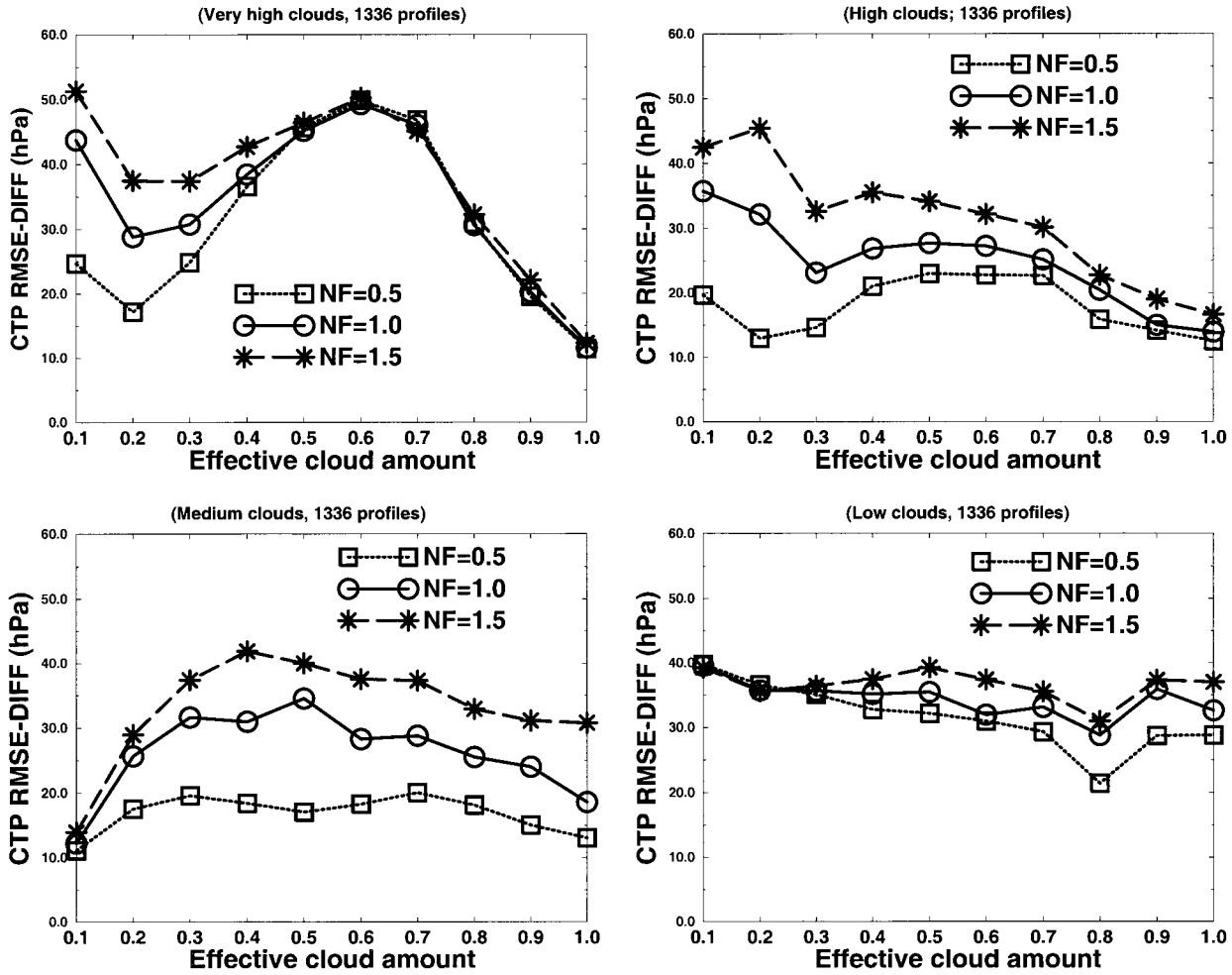


FIG. 9. The RMSE-DIFF between $CO_2$ slicing and 1DVAR (rmse of $CO_2$ slicing minus rmse of 1DVAR) for CTP with different instrument noise factors (0.5, 1.0, and 1.5, respectively).

radiances for thick, high clouds is significantly greater than the instrument noise level; therefore, a noise factor of 0.5 or 1.5 will not have much influence on the retrievals from both $CO_2$ slicing and 1DVAR. For medium clouds (lower left), high instrument noise results in a large improvement (15–40 hPa) and low instrument noise gives less improvement (10–20 hPa) for all possible ECA. For low clouds (lower right), the noise impact on the 1DVAR improvement over $CO_2$ slicing is small; 1DVAR gives similar improvement over $CO_2$ slicing with three different instrument noise factors. Because the cloud retrieval is based on the window technique for low clouds and the noise for window band is small (see Table 1), a noise factor of 0.5 or 1.5 does not have much change on the window technique cloud retrieval as well as the 1DVAR cloud retrieval, which is based on the low-level bands also with small instrument noise level.

Figure 10 shows the RMSE-DIFF between $CO_2$ slicing and 1DVAR for the ECA with three different instrument noise factors (0.5, 1.0, and 1.5, respectively). Because ECA is derived from the window band with a low instrument noise, the influence of instrument noise (noise factor of 0.5 or 1.5) on the 1DVAR improvement over $CO_2$ slicing for ECA is relatively small, although the improvement with large instrument noise is greater than that with low instrument noise for most types of cloud.

## 6. Comparisons between the $CO_2$-slicing and 1DVAR cloud retrievals from the *GOES-8* sounder cloudy radiance measurements

The GOES cloud retrieval procedure involves several steps that include the following: (a) identify clear versus cloudy FOV by intercomparing brightness temperatures in adjacent $CO_2$ bands (Hayden et al. 1988), (b) apply a radiance bias adjustment to account for the clear-sky measured-versus-calculated radiance differences (c) apply the $CO_2$-slicing and 1DVAR algorithms to each cloudy single FOV within a field of regard (FOR) (hereinafter, we define an FOR as a $3 \times 3$ FOV area), and

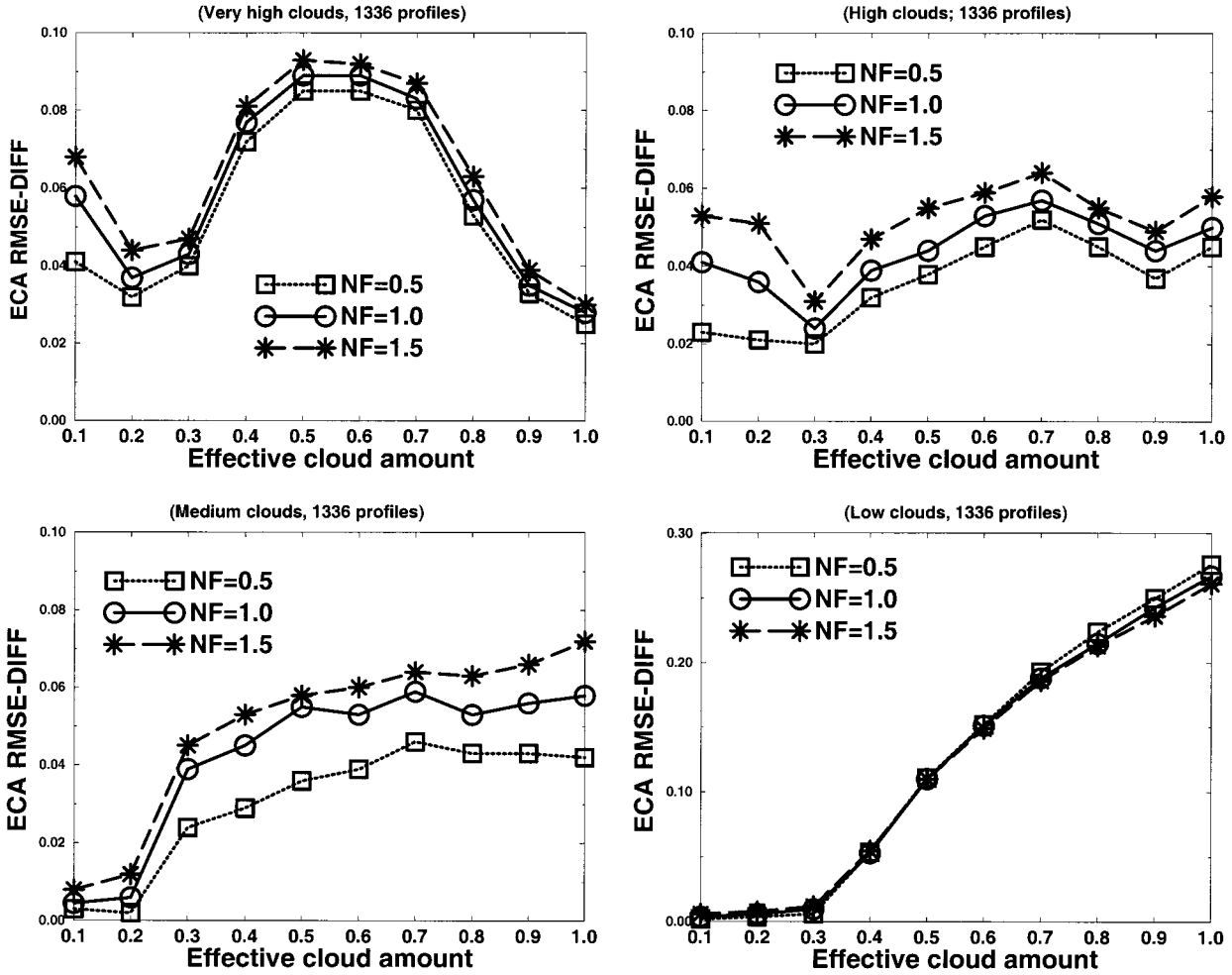


FIG. 10. The RMSE-DIFF between $CO_2$ slicing and 1DVAR for ECA with different instrument noise factors (0.5, 1.0, and 1.5, respectively).

(d) average the CTPs and ECAs from an FOR to represent the cloud retrievals for this FOR. The $CO_2$-slicing and 1DVAR retrieval procedures will be performed only if one or more cloudy FOVs are detected within an FOR. The averaging is weighted by the ECA of each cloudy FOV within the FOR. In the GOES sounder data processing, one IR surface emissivity for the longwave bands was retrieved simultaneously with the atmospheric profile for clear-sky conditions (Hayden 1988). For cloudy-sky conditions, assuming the local variation of IR surface emissivity is small, the nearby clear-sky IR emissivity was used for the cloud retrievals. The assumption of uniform IR surface emissivity might be a source of error, depending on the local variability of surface emissivities but it is not the main source of error in the $CO_2$-slicing and 1DVAR cloud retrievals when compared with other error sources such as instrument noise, temperature profile, and surface skin temperature.

The atmospheric profile and surface skin temperature are obtained from NCEP's forecast analysis and NWSs hourly surface observations, respectively. In 1DVAR iteration, convergence was checked by

$$\chi_i = |X_i - X_{i-1}|. \tag{14}$$

If $\chi_{i+1}$ is greater than $\chi_i$ within two iterations (which means the iteration diverges), then the iteration is stopped, and the retrieval is set to the $CO_2$-slicing background. Otherwise the iteration continues until $\chi$ is less than 0.5 or a maximum of five iterations is reached. In each iteration, CTP is limited to 115 hPa for the highest and 1013 hPa for the lowest, and ECA must be less than or equal to 1.0 and greater than or equal to zero. In addition, if the residual brightness temperatures for all the longwave spectral bands (except band 1) calculated from the $CO_2$-slicing-derived CTP and ECA are less than 2 times the instrument noise level, the 1DVAR will not be attempted. Statistics based on single cloudy FOV retrievals were calculated to sort out the number of successful 1DVAR retrievals. A total of 24 000 cloudy FOVs were found for the $CO_2$-slicing retrieval.

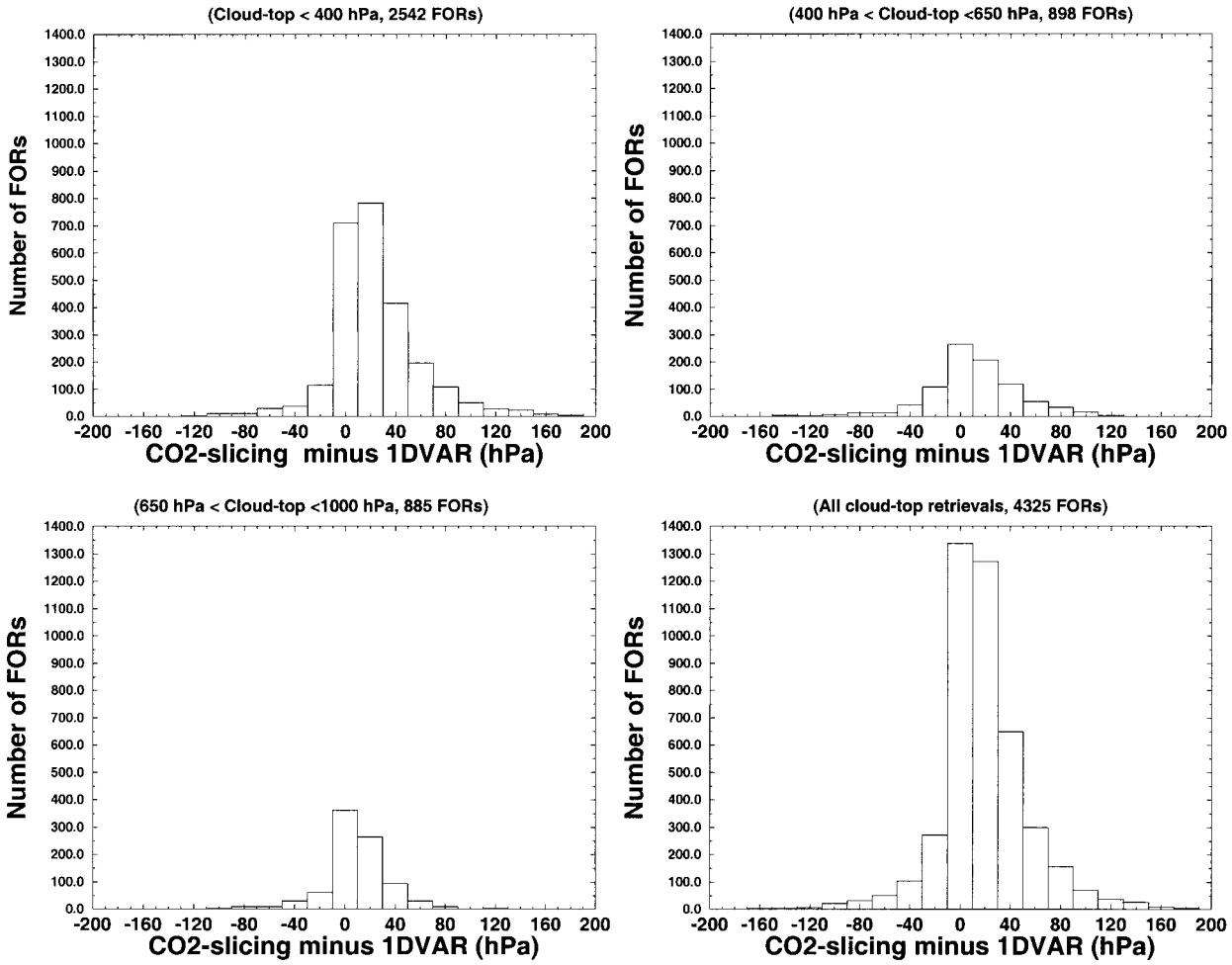


FIG. 11. The histograms of differences between CTPs as retrieved from the $CO_2$-slicing and 1DVAR algorithms for four cloud types at 2346 UTC 6 Oct 1999. The four cloudy types based on the 1DVAR retrievals are the clouds above 400 hPa, clouds between 400 and 650 hPa, clouds between 650 and 1000 hPa, and all of the clouds together.

The 1DVAR algorithm was not performed for 4800 (20%) of these FOVs because of the small residual between measured and calculated (from the $CO_2$-slicing cloud background) brightness temperatures. A total of 18 240 (76%) FOVs were successfully convergent; 960 (4%) were divergent.

In the following comparisons, only FORs with successful 1DVAR performance were included. Figure 11 shows the histograms of differences between CTPs as retrieved from the $CO_2$-slicing and 1DVAR algorithms for four cloud types at 2346 UTC 6 October 1999. The longwave spectral-band images are shown in Fig. 2. The four cloudy types based on the 1DVAR retrievals are the clouds above 400 hPa, clouds between 400 and 650 hPa, clouds between 650 and 1000 hPa, and all the clouds together. It can be seen that most clouds occurred as high clouds (upper left); the distribution of the differences ($CO_2$ minus 1DVAR) is asymmetric, with more positive differences for all levels of clouds. This result means that the $CO_2$ slicing assigned lower clouds than did 1DVAR. For high clouds and low clouds in particular, more positive differences were found, in agreement with the simulation results shown in Fig. 4. Comparisons between the $CO_2$ slicing and the pilot cloud reports also show that $CO_2$ slicing assigned lower clouds (SSM).

Figure 12 shows the *GOES-8* window band (band 8) image of clouds near the Florida coastline. The $CO_2$-slicing-derived CTPs and ECAs (upper left and upper right) and 1DVAR CTPs and ECAs (lower left and lower right) are shown. CTP is averaged only from cloudy FOVs, and the ECA is averaged from all $3 \times 3$ FOVs within each FOR. Most clouds appear at high levels in this scene; the pressure levels from $CO_2$ slicing are lower than those from 1DVAR. These results are consistent with the simulation shown in Fig. 4 (upper left and right panels).

Figure 13 shows the rms for residual of eight longwave spectral bands from the $CO_2$-slicing and 1DVAR cloud retrievals. The residual is defined as the difference

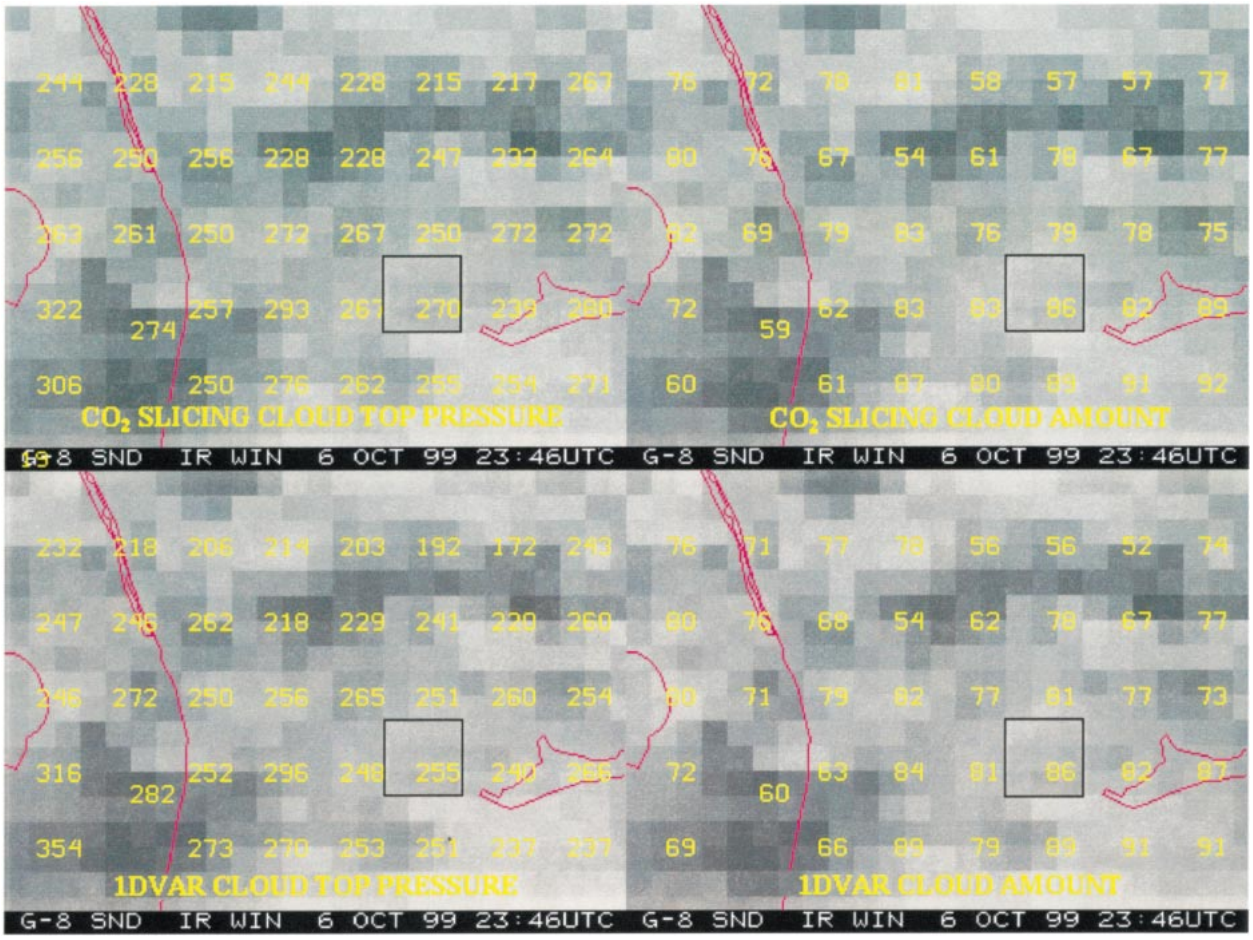


FIG. 12. The *GOES-8* window band (band 8) image, which depicts the clouds in the Florida coastline, with the $CO_2$-slicing–derived CTPs and ECAs (upper left and upper right) and 1DVAR CTPs and ECAs (lower left and lower right) at 2346 UTC 6 October 1999. The black box in each of the four panels represents a $3 \times 3$ box (or one FOR). The CTP is averaged from the cloudy FOVs while the ECA is averaged from $3 \times 3$ FOVs within each FOR. The units are hPa and % for CTP and ECA, respectively, in this figure.

between the observed and the calculated brightness temperatures. Band 1 has no residual change, and bands 2 and 3 have only slight changes. For the other bands, the residual brightness temperatures for 1DVAR are significantly reduced by 0.6–0.9 K from those for $CO_2$ slicing. This result indicates that the cloud information for most FOVs is not fully used in $CO_2$ slicing; the 1DVAR is better able to fit the cloudy measurements by changing the $CO_2$-slicing CTP and ECA.

## 7. Discussion

Why does the 1DVAR enable an improvement over $CO_2$ slicing? Three possible factors are involved. First, $CO_2$ slicing uses only two spectral bands to extract information for a given cloud. Also, bands 2 and 3 are not used in $CO_2$ slicing. However, 1DVAR simultaneously uses all the longwave spectral bands weighted by the observation error to retrieve the cloud information.

Second, $CO_2$ slicing uses a ratio to obtain the cloud-top pressure, and the ratio may be sensitive to the observation error or other uncertainties, such as inaccurate temperature profiles in the radiative transfer calculation. Error in the ratio may amplify the error of the $CO_2$-slicing cloud-top pressure (as shown in Figs. 9 and 10). Because 1DVAR uses all weighted longwave spectral-band cloudy radiances, it is possible to reduce the error in $CO_2$ slicing resulting from the error of the satellite measurements or uncertainties in the radiative transfer calculation.

Third, 1DVAR uses a penalty function to measure the degree of fit of the cloudy measurements to the $CO_2$-slicing cloud information. The solution will provide a balance between longwave sounder cloudy radiances and the $CO_2$-slicing background. The 1DVAR solution of Eq. (9) has the following important characteristics. If the $CO_2$ slicing was good quality (it fits all the longwave spectral-band cloudy radiances well), less weight is given to the satellite measurements in the 1DVAR iteration, and the solution will be only a slight modification of $CO_2$-slicing-derived CTP and ECA. How-

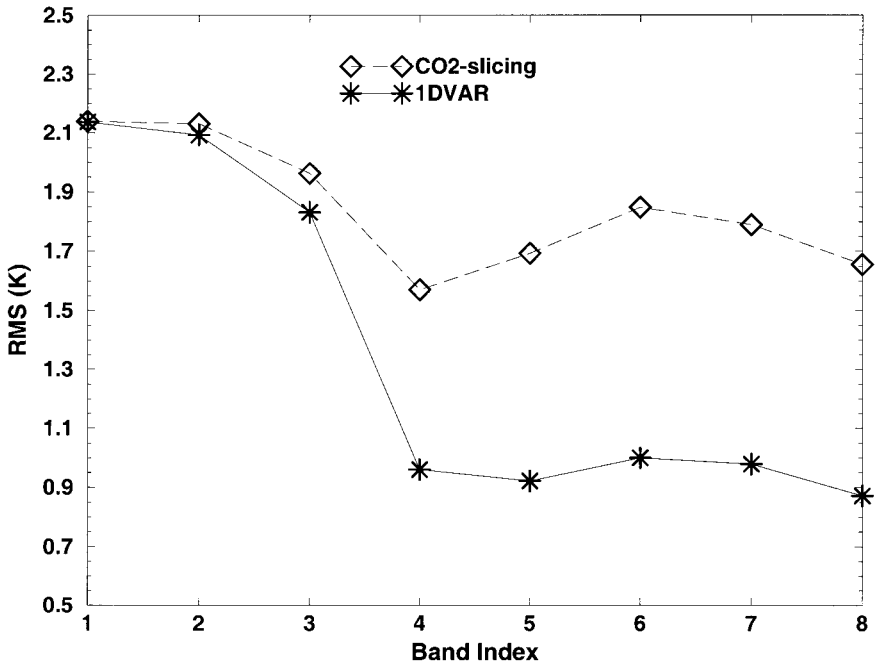


FIG. 13. The rms for residual between measured and calculated brightness temperatures of eight longwave spectral bands from the $CO_2$-slicing and 1DVAR cloud retrievals at 2346 UTC 6 Oct 1999.

ever, if the $CO_2$-slicing-derived CTP and ECA do not fit all the longwave spectral band cloudy radiances, then a large weight will be given to the 1DVAR-retrieved cloud parameters. Thus, the $CO_2$-slicing cloud parameters will be heavily modified to obtain the best simultaneous fit to all the longwave bands.

How does 1DVAR change the $CO_2$-slicing-derived cloud background in the iteration procedure? The change is highly dependent on the residual brightness temperatures calculated from the $CO_2$-slicing cloud background. If the initial residual brightness temperature $[R^m - R(\mathbf{X}_0)]$ for any cloud-sensitive longwave spectral bands is significantly larger than its instrument noise (see Fig. 13), a change of the $CO_2$-slicing CTP and ECA is expected in 1DVAR through minimizing the penalty function of Eq. (3).

Figure 14 presents an example showing the variation of the *GOES-8* longwave spectral-band residual brightness temperature after the first two iterations (the penalty function is shown in Fig. 3). Band 1 has no cloud information, and there is almost no residual change for band 1 during the iterations. Residual changes for bands 3–6 are large in the iterations for this particular case of medium cloud. The initial residual brightness temperatures for most bands are larger than the *GOES-8* instrument noise, and they are reduced significantly in the first two iterations.

Figure 15 shows the associated CTP and ECA variations after the first two iterations. The background CTP and the ECA are 350 hPa and 0.36 from $CO_2$ slicing. After two iterations, it tends to the truth of 500 hPa for CTP and 0.5 for ECA. However, if the $CO_2$-slicing-derived CTP and ECA make the initial residual brightness temperatures small for all longwave spectral bands, the 1DVAR retrieval procedure will not be performed, because the $CO_2$ slicing already fits the longwave spectral-band cloudy radiance measurements.

## 8. Conclusions and future extensions

A two-step procedure ($CO_2$ slicing followed by 1DVAR) is described in this paper for cloud retrievals from the *GOES-8* sounder longwave spectral-band cloudy radiance measurements. The CTP and ECA derived from the $CO_2$-slicing technique are used as the background in the 1DVAR retrieval processing. Simulation studies with global datasets were carried out to investigate the accuracy of CTPs and ECAs derived from both the $CO_2$-slicing and 1DVAR algorithms; significant improvement of 1DVAR over the $CO_2$-slicing technique is found. Also, *GOES-8* sounder cloudy radiance measurements were processed, and the derived CTPs from $CO_2$ slicing were compared with the 1DVAR cloud retrievals. The following conclusions can be drawn (conclusions 1–4 were from simulations and 5–6 were from inversion of *GOES-8* cloudy radiance measurements).

1) An improvement of 10–50 hPa of rmse was found in 1DVAR over $CO_2$ slicing for most high clouds; this improvement results from the reduction of bias in 1DVAR retrievals over $CO_2$ slicing.

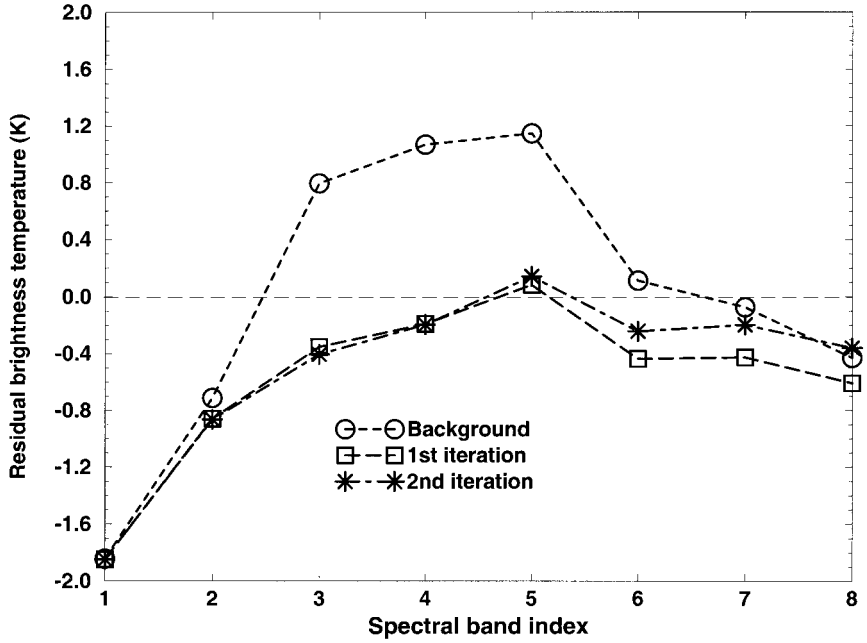


FIG. 14. An example showing the *GOES-8* longwave spectral-band residual brightness temperature variations after the first two iterations (the penalty function is shown in Fig. 3).

2) A systematic improvement of rmse was seen in 1DVAR for medium clouds over the $CO_2$ slicing, ranging from 10 to 35 hPa, depending on ECA.
3) An improvement of 35 hPa of rmse was found in 1DVAR for low clouds over $CO_2$ slicing; this improvement is also due to the reduction of bias in 1DVAR.
4) The improvement of 1DVAR over $CO_2$ slicing is sensitive to instrument noise for thin, high clouds and all medium clouds. High instrument noise will

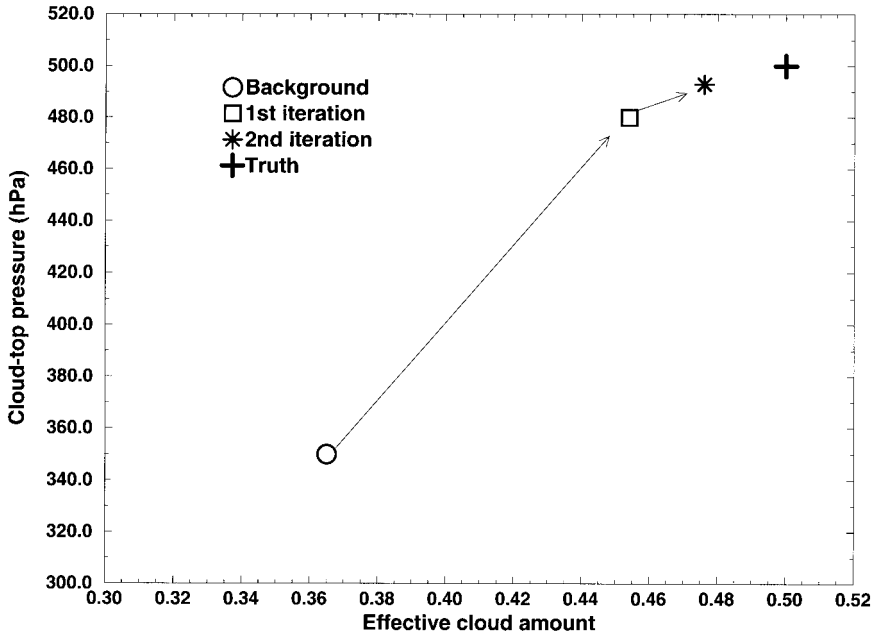


FIG. 15. The associated CTP and ECA variations after the first two iterations (the variation for residual brightness temperatures is shown in Fig. 14). The background CTP and ECA are assumed to be 350 hPa and 0.36 from the $CO_2$-slicing algorithm.

result in a large improvement in 1DVAR; low instrument noise gives less improvement in 1DVAR for those clouds.
5) $CO_2$ slicing assigned clouds to be lower than 1DVAR did for high and low clouds.
6) The cloud information for most cloudy FOVs is not fully used in $CO_2$ slicing; 1DVAR is able to fit the cloudy measurements better by modifying the $CO_2$-slicing CTP and ECA.

By using simulated data, it is possible to compare the behavior of the $CO_2$-slicing and 1DVAR performances against true cloud properties. However, real validation will depend on other sources of cloud measurements such as lidar and ground observations; this approach is under consideration. Additional work must also focus on cloud retrievals under the conditions of low-level temperature inversions as well as multilayer clouds. Multilayer clouds are a physical reality that will be considered in future work using the high-spectral-resolution sounders such as Geostationary Imagery Fourier Transform Spectrometer (a description was available at the time of writing online at http://danspc.larc.nasa.gov/GIFTS/) measurements. The effect of the $CO_2$-slicing and 1DVAR cloud retrievals on numerical weather prediction should also be investigated.

*Acknowledgments.* The authors are grateful to Timothy J. Schmit, who provided invaluable help in the GOES sounder data processing. Thanks are also due to Drs. John R. Eyre and Hung-Lung Huang for the helpful discussions on the cloud retrieval algorithms. Two anonymous reviewers' comments were of considerable help in improving the text. Christopher C. Sisko provided Fig. 3 for this paper. This research was supported by NOAA Grant NA67 EC00100.

## APPENDIX

### Linearization of Cloudy Radiative Transfer Equation

Using the symbols defined in section 2, the theoretical upwelling radiance $R$ for a partially cloud-filled FOV is given by

$$R = (1 - N\varepsilon_c)R_{\text{clr}} + N\varepsilon_c R_{\text{cld}}, \tag{A1}$$

where

$$R_{\text{clr}} = \varepsilon_s B_s \tau_s - \int_0^{p_s} B\, d\tau(0, p) + (1 - \varepsilon_s) \int_0^{p_s} B\, d\tau^* \quad \text{and} \tag{A2}$$

$$R_{\text{cld}} = B_c \tau_c - \int_0^{p_c} B\, d\tau(0, p). \tag{A3}$$

The linearized form of Eq. (A1) with respect to the cloud-top pressure and the effective cloud amount is obtained as

$$\delta R = (R_{\text{cld}} - R_{\text{clr}})\delta(N\varepsilon_c) + (N\varepsilon_c)\frac{\partial R_{\text{cld}}}{\partial p_c}\delta p_c. \tag{A4}$$

Because

$$\frac{\partial R_{\text{cld}}}{\partial p_c} = B_c\frac{\partial \tau_c}{\partial p_c} + \tau_c\frac{\partial B_c}{\partial p_c} - \frac{\partial\left(\int_0^{p_c} B\frac{\partial \tau}{\partial p}\, dp\right)}{\partial p_c} \tag{A5}$$

and

$$\frac{\partial\left(\int_0^{p_c} B\frac{\partial \tau}{\partial p}\, dp\right)}{\partial p_c} = B_c\frac{\partial \tau_c}{\partial p_c}, \tag{A6}$$

substitute Eq. (A6) into Eq. (A5), and we have

$$\frac{\partial R_{\text{cld}}}{\partial p_c} = \tau_c\frac{\partial B_c}{\partial p_c}. \tag{A7}$$

Substitute Eq. (A7) into Eq. (A4) and the linearized form is obtained

$$\delta R = (R_{\text{cld}} - R_{\text{clr}})\delta(N\varepsilon_c) + (N\varepsilon_c)\tau_c\frac{\partial B_c}{\partial p_c}\delta p_c. \tag{A8}$$

## REFERENCES

Baum, B. A., and B. A. Wielicki, 1994: Cirrus cloud retrieval using infrared sounder data: Multilevel cloud errors. *J. Appl. Meteor.*, **33,** 107–117.

Bayler, G. M., R. M. Aune, and W. H. Raymond, 2000: NWP cloud initialization using GOES sounder data and improved modeling of nonprecipitating clouds. *Mon. Wea. Rev.,* **128,** 3911–3920.

Chahine, M. T., 1974: Remote sounding of cloudy atmospheres. I. The single layer cloud. *J. Atmos. Sci.,* **31,** 233–243.

Diak, G. R., M. C. Anderson, W. L. Bland, J. M. Norman, J. M. Mecikalski, and R. A. Aune, 1998: Agricultural management decisions aids driven by real-time satellite data. *Bull. Amer. Meteor. Soc.,* **79,** 1345–1355.

Eyre, J. R., 1989: Inversion of cloudy satellite sounding radiances by nonlinear optimal estimation. I: Theory and simulation. *Quart. J. Roy. Meteor. Soc.,* **115,** 1001–1026.

——, and W. P. Menzel, 1989: Retrieval of cloud parameters from satellite sounder data: A simulation study. *J. Appl. Meteor.,* **28,** 267–275.

Frey, R. A., B. A. Baum, W. P. Menzel, S. A. Ackerman, C. C. Moeller, and J. D. Spinhirne, 1999: A comparison of cloud top heights computed from airborne lidar and MAS radiance data using $CO_2$ slicing. *J. Geophys. Res.,* **104,** 24 547–24 555.

Hannon, S., L. L. Strow, and W. W. McMillan, 1996: Atmospheric infrared fast transmittance models: A comparison of two approaches. *Proc. SPIE,* **2830,** 94–105.

Hayden, C. M., 1988: GOES-VAS simultaneous temperature–moisture retrieval algorithm. *J. Appl. Meteor.,* **27,** 705–733.

Isaacs, R. G., R. N. Hoffman, and L. D. Kaplan, 1986: Satellite remote sensing of meteorological parameters for global numerical weather prediction. *Rev. Geophys.,* **24,** 701–743.

Kim, D. S., and S. G. Benjamin, 2000: Assimilation of cloud-top pressure derived from GOES sounder data into MAPS/RUC.

Preprints, *10th Conf. on Satellite Meteorology and Oceanography*, Long Beach, CA, Amer. Meteor. Soc., 110–113.

Li, J., and H. L. Huang, 1999: Retrieval of atmospheric profiles from satellite sounder measurements using the discrepancy principle. *Appl. Opt.*, **38,** 916–923.

——, W. Wolf, W. P. Menzel, W. Zhang. H.-L. Huang, and T. H. Achtor, 2000: Global soundings for the atmosphere from ATOVS measurements: The algorithm and validation. *J. Appl. Meteor.*, **39,** 1248–1268.

——, C. C. Schmidt, J. P. Nelson, T. J. Schmit, and W. P. Menzel, 2001: Estimation of total ozone from GOES sounder radiances with high temporal resolution. *J. Atmos. Oceanic Technol.*, **18,** 157–168.

Menzel, W. P., and J. F. W. Purdom, 1994: Introducing GOES-I: The first of a new generation of geostationary operational environmental satellites. *Bull. Amer. Meteor. Soc.*, **75,** 757–781.

——, W. L. Smith, and T. R. Stewart, 1983: Improved cloud motion wind vector and altitude assignment using VAS. *J. Climate Appl. Meteor.*, **22,** 377–384.

——, D. P. Wylie, and K. I. Strabala, 1992: Seasonal and diurnal changes in cirrus clouds as seen in four years of observations with VAS. *J. Appl. Meteor.*, **31,** 370–385.

——, F. C. Holt, T. J. Schmit, R. M. Aune, A. J. Schreiner, G. S. Wade, and D. G. Gray, 1998: Application of *GOES-8/9* soundings to weather forecasting and nowcasting. *Bull. Amer. Meteor. Soc.*, **79,** 2059–2077.

Rodgers, C. D., 1976: Retrieval of atmospheric temperature and composition from remote measurements of thermal radiation. *Rev. Geophys. Space Phys.*, **14,** 609–624.

Schreiner, A. J., D. A. Unger, W. P. Menzel, G. P. Ellrod, K. I. Strabala, and J. L. Pellet, 1993: A comparison of ground and satellite observations of cloud cover. *Bull. Amer. Meteor. Soc.*, **74,** 1851–1861.

Smith, W. L., and C. M. R. Platt, 1978: Intercomparison of radiosonde, ground-based laser, and satellite-deduced cloud heights. *J. Appl. Meteor.*, **17,** 1796–1802.

——, and R. A. Frey, 1990: On cloud altitude determinations from high-resolution interferometer sounder (HIS) observations. *J. Appl. Meteor.*, **29,** 658–662.

——, H. M. Woolf, P. G. Abel, C. M. Hayden, M. Chalfant, and N. Grody, 1974: *Nimbus-5* sounder data processing system. Part I: Measurement characteristics and data reduction procedures. NOAA Tech. Memo. NESS 57, 99 pp. [Available from National Technical Information Service, 5285 Port Royal Rd., Springfield, VA 22161.]

——, ——, C. M. Hayden, D. C. Wark, and L. M. McMillin, 1979: *TIROS-N* operational vertical sounder. *Bull. Amer. Meteor. Soc.*, **60,** 1177–1187.

——, ——, ——, and A. J. Schreiner, 1985: The simultaneous export retrieval package. *Tech. Proc. Second Int. TOVS Study Conf.*, Igls, Austria, International TOVS Working Group, 224–253. [Available from Schwerdtfeger Library, University of Wisconsin—Madison, 1225 West Dayton Street, Madison, WI 53706.]

Stephens, G. L., and P. J. Webster, 1981: Clouds and climate: Sensitivity of simple systems. *J. Atmos. Sci.*, **38,** 235–247.

——, S. C. Tsay, J. P. W. Stackhouse, and P. Flatau, 1990: The relevance of the microphysical and radiative properties of cirrus clouds to climate and climatic feedback. *J. Atmos. Sci.*, **47,** 1742–1753.

Susskind, J., J. Rosenfield, D. Reuter, and M. T. Chahine, 1984: Remote sensing of weather and climate parameters from HIRS2/MSU on *TIROS-N*. *J. Geophys. Res.*, **89,** 4677–4697.

——, D. Reuter, and M. T. Chahine, 1987: Cloud fields retrieved from analysis of HIRS2/MSU sounding data. *J. Geophys. Res.*, **92,** 4035–4050.

Velden, C. S., C. M. Hayden, S. J. Nieman, W. P. Menzel, S. Wanzong, and J. S. Goerss, 1997: Upper-tropospheric winds derived from geostationary satellite water vapor observations. *Bull. Amer. Meteor. Soc.*, **78,** 173–195.

Wielicki, B. A., and J. A. Coakley Jr., 1981: Cloud retrieval using infrared sounder data: Error analysis. *J. Appl. Meteor.*, **20,** 157–169.

Wu, X., W. P. Menzel, and G. S. Wade, 1999: Estimation of sea surface temperature using *GOES-8/9* radiance measurements. *Bull. Amer. Meteor. Soc.*, **80,** 1127–1138.

Wylie, D. P., and W. P. Menzel, 1989: Two years of cloud cover statistics using VAS. *J. Climate*, **2,** 380–292.

——, and ——, 1999: Eight years of high-cloud statistics using HIRS. *J. Climate*, **12,** 170–184.